PUBLICATIONS OF
THE UNIVERSITY OF EASTERN FINLAND

*Dissertations in Forestry and Natural Sciences*


RIZWAN ALI

# FABRICATION OF THIN FILMS AND OPTICAL NANOSTRUCTURES BY ATOMIC LAYER DEPOSITION

UNIVERSITY OF
EASTERN FINLAND

PUBLICATIONS OF THE UNIVERSITY OF EASTERN FINLAND
DISSERTATIONS IN FORESTRY AND NATURAL SCIENCES

No 337

*Rizwan Ali*

# FABRICATION OF THIN FILMS AND OPTICAL NANOSTRUCTURES BY ATOMIC LAYER DEPOSITION

ACADEMIC DISSERTATION

To be presented by the permission of the Faculty of Science and Forestry for public examination in the Auditorium M103 in Metria Building at the University of Eastern Finland, Joensuu, on April 26, 2019, at 12 o'clock noon.

University of Eastern Finland
Institute of Photonics
Joensuu 2019

Grano Oy
Jyväskylä, 2019
Editors: Pertti Pasanen, Jukka Tuomela,
Matti Tedre, and Raine Kortet

Distribution:
University of Eastern Finland Library / Sales of publications
julkaisumyynti@uef.fi
http://www.uef.fi/kirjasto

ISBN: 978-952-61-3036-1 (print)
ISSNL: 1798-5668
ISSN: 1798-5668
ISBN: 978-952-61-3037-8 (pdf)
ISSNL: 1798-5668
ISSN: 1798-5676

Author's address:
University of Eastern Finland
Institute of Photonics
P.O. Box 111
80101 JOENSUU
FINLAND
email: rizwan.ali@uef.fi

Supervisors:
Professor Seppo Honkanen
University of Eastern Finland
Institute of Photonics
P.O. Box 111
80101 JOENSUU
FINLAND
email: seppo.honkanen@uef.fi

Professor Jari Turunen
University of Eastern Finland
Institute of Photonics
P.O. Box 111
80101 JOENSUU
FINLAND
email: jari.turunen@uef.fi

Professor Muhammad Rizwan Saleem
National University of Sciences and Technology (NUST)
U.S.-Pakistan Center for Advanced Studies in Energy
P.O. Box 44000
Sector H-12, ISLAMABAD
PAKISTAN
email: rizwan@casen.nust.edu.pk

Reviewers:
Professor Ilkka Tittonen
Aalto University
Department of Electronics and Nanoengineering
Tietotie 3
02015 ESPOO
FINLAND
email: ilkka.tittonen@aalto.fi

Associate Professor Benfeng Bai
Tsinghua University
Department of Precision Instrument
P.O. Box 100084
Haidian District, BEIJING
P.R. CHINA
email: baibenfeng@tsinghua.edu.cn

Opponent:
Dr. Toralf Scharf
École Polytechnique Fédérale de Lausanne (EPFL)
Nanophotonics and Metrology Laboratory
EPFL STI IMT NAM
ELG 237 (Bâtiment ELG) Station 11
CH-1015 LAUSANNE
SWITZERLAND
email: toralf.scharf@epfl.ch

Rizwan Ali
Fabrication of Thin Films and Optical Nanostructures by Atomic Layer Deposition
Joensuu: University of Eastern Finland
Publications of the University of Eastern Finland
Dissertations in Forestry and Natural Sciences 2019; 337

## ABSTRACT

The research work described and demonstrated in this thesis is about exploring qualitatively and quantitatively the thermo-optical properties of thin films fabricated by atomic layer deposition (ALD) and characterized by spectroscopic ellipsometry. At first, the negative thermo-optical behavior of titanium dioxide ($TiO_2$) thin films, which is the main reason for optical device malfunctionality at higher temperatures, is controlled by the use of over-layer aluminum oxide ($Al_2O_3$) thin films. The use of $Al_2O_3$ thin films on top of $TiO_2$ thin films helps to stabilize the optical properties of such films at higher temperatures and the bilayer combinations of such films further pave the way for athermal operation of the optical devices at elevated temperatures. This thesis also reports on a theoretical and experimental study of sub-wavelength guided mode resonance filters, designed by Fourier Modal Method (FMM), fabricated by electron beam lithography and reactive ion etching, buried by ALD-$TiO_2$ thin films, and characterized optically by spectroscopic ellipsometry for sensing applications.

***Universal Decimal Classification:*** *535.3, 535.4, 536.4, 620.3, 681.7.02*
***Keywords:*** *light; optics; photonics; thin films; titanium dioxide; aluminum oxide; optical properties; thermal properties; buried gratings; sensing; nano-fabrication; electron beam lithography; reactive ion etching; atomic layer deposition; spectroscopic ellipsometry; X-ray diffractometry; atomic force microscopy; scanning electron microscopy*

## ACKNOWLEDGEMENTS

First of all I wish to express my utmost gratitude to my supervisors Prof. Seppo Honkanen, Prof. Jari Turunen and Prof. Muhammad Rizwan Saleem for provision of the best research opportunities, funding, encouragement, and all kind of support during my M.Sc. and Ph.D. studies.

I would like to acknowledge the head of the Department of Physics and Mathematics and the director of Institute of Photonics, Prof. Jyrki Saarinen, for providing me the excellent platform for research work. I am deeply thankful to Assoc. Prof. Matthieu Roussey, for his valuable discussions, sustaining and increasing my research interest, important contributions to my research work, and accepting to be the custos. I would like to thank the reviewers Prof. Ilkka Tittonen and Assoc. Prof. Benfeng Bai for their insightful comments and suggestions during my thesis review process. I am humbly grateful to Dr. Toralf Scharf for accepting to be the opponent. I extend my heartiest appreciations to all the co-authors for their undivided attention and contributions to my research work.

I am specially thankful to Dr. Janne Laukkanen, Dr. Pertti Pääkkönen, Tommi Itkonen, and Timo Vahimaa for providing cleanroom training, their humble and always ready-to-help nature. I owe my special thanks to Ms. Hannele Karppinen, Ms. Katri Mustonen, Ms. Noora Heikkilä, Ms. Marita Ratilainen, and Ms. Oili Kohonen for their kind support to all administrative tasks during all my years at UEF. I am extremely grateful to professors, lecturers, post docs., and colleagues for their help and meaningful discussions during my Ph.D. studies. I would further like to thank all of my friends in Finland, Pakistan and abroad who kept me uplifted in my studies.

Last, but certainly not the least, it is the best moment to offer my deepest gratefulness to my family who relentlessly encouraged me throughout my academic journey.

Joensuu, April 26, 2019

*Rizwan Ali*

## LIST OF PUBLICATIONS

This thesis consists of the present review of the author's work in the field of thin films and optical nanostructures and the following selection of the author's publications:

**I** M. R. Saleem, **R. Ali**, S. Honkanen, J. Turunen, "Thermal properties of thin $Al_2O_3$ films and their barrier layer effect on thermo-optic properties of $TiO_2$ films grown by atomic layer deposition," *Thin Solid Films* **542**, 257–262 (2013).

**II** **R. Ali**, M. R. Saleem, P. Pääkkönen and S. Honkanen, "Thermo-Optical Properties of Thin-Film $TiO_2$–$Al_2O_3$ Bilayers Fabricated by Atomic Layer Deposition," *Nanomaterials* **5**, 792–803 (2015).

**III** **R. Ali**, M. R. Saleem, M. Roussey, J. Turunen & S. Honkanen, "Fabrication of buried nanostructures by atomic layer deposition," *Sci. Rep.* **8**, 15098 (2018).

Throughout the overview, these papers will be referred to by Roman numerals. (Other publications and contributions by the author are listed in the appendix).

## AUTHOR'S CONTRIBUTION

The publications selected in this dissertation are original research papers published as a result of collective efforts by the author and co-authors. The author has performed the optical measurements for Paper [**I**]. The author has contributed to the fabrication, measurements, and the characterization of the thin-film structures reported in Paper [**II**]. In Paper [**III**], the author has designed the structures by numerical simulations, fabricated the structures, and performed the optical measurements. The author has participated actively in writing of all the papers. The cooperation with the co-authors has been significant in all the papers.

# TABLE OF CONTENTS

# 1 Introduction

In a variety of optoelectronic and photonic devices, the ability to withstand harsh operating conditions without affecting the output is generally required to increase the operating flexibility and functionality of the device. Such systems often contain thin optical films or diffractive elements (e.g., diffraction gratings), or combinations of both [1], depending on the desired optical function. The incorporation of thin films, diffraction gratings, and other nano-optical elements makes it important to study their functionality in varying environments.

There exists a huge variety of thin films that are being used in optics and photonics, based on their individual optical properties and functionalities. Among these films, $TiO_2$ thin films are an excellent choice to be used as cover layers in a variety of devices owing to their high refractive index, thermal stability, high transparency and low loss in the visible (VIS) and infrared (IR) regions of the electromagnetic spectrum [2]. Due to these desirable optical properties, $TiO_2$ thin films are widely used in nano-optical devices for numerous applications [3]. Unfortunately, the optical properties of these films are affected greatly by the surrounding environmental conditions, including temperature, humidity, and moisture. Such environmental variations may significantly alter the device functionality, especially when the film thickness is in the range of a few tens of nanometers. Hence a comprehensive study of the optical properties of $TiO_2$ thin films of various thicknesses in different operating environments (e.g., temperature in our case), and devising ways to thermally stabilize these properties, is generally important.

It has been found that temperature variations lead to the changes in the refractive index and thickness of $TiO_2$ films fabricated by Atomic Layer Deposition (ALD). These changes are characterized by the thermo-optic coefficient (TOC) $\mathrm{d}n/\mathrm{d}T$ and the density coefficient $\mathrm{d}\rho(T)/\mathrm{d}T$. In particular, it has been established that $TiO_2$ thin films with thickness below 150 nm are more prone than thicker layers to temperature-dependent optical changes due to surface porosity effects that allow water vapor permeation. As a result, thin films exhibit negative TOCs, whereas thicker films (thickness $>$ 150 nm) possess positive TOCs [4]. In many device applications, thin $TiO_2$ films (thickness $<$ 150 nm) are nevertheless employed. As a result, the thermal stability of the optical properties of such films is a prerequisite for stable device operation in temperature varying conditions.

High thermal stability in optical properties of thin $TiO_2$ films can be achieved by employing, e.g., $Al_2O_3$ diffusion barrier films on the $TiO_2$ films. Such $Al_2O_3$ films exhibit natural immunity to environmental variations, and they also have excellent optical properties [5–10]. The idea behind utilizing $Al_2O_3$ barrier films is to protect the underlying $TiO_2$ films while retaining their inherent optical properties so as to ensure proper and stable operation of optical devices in varying temperature conditions. In fact, after exploration of thermo-optic properties of $TiO_2$ films, it is intrinsically required to study the properties of $Al_2O_3$ barrier films of similar thicknesses in varying temperature conditions in order to validate this idea.

It is shown in Paper **I** that the use of $Al_2O_3$ barrier films in the form of $TiO_2$–$Al_2O_3$ bilayers helps to protect the underlaying $TiO_2$ films and improve their in-

herent optical properties over a wide temperature range ($T$ = 20–150°C) in terms of TOCs. In general, the optical properties and structural morphologies of thin films are greatly influenced by thin film deposition techniques and process methods [4,11,12]. The influence of environmental effects (namely temperature) on the optical properties of $TiO_2$ and $Al_2O_3$ thin films, and $TiO_2$–$Al_2O_3$ bilayer films, is studied experimentally in Papers **I** and **II**. Thin ($\sim$ 100 nm) $TiO_2$ films and $Al_2O_3$ barrier films are studied in various bilayer combinations with the aim to achieve nearly athermal operation with positive TOCs. This has been nearly achieved. Furthermore, in addition to the work presented here, preliminary studies on thermo-optical and different crystalline phase properties of ALD-$TiO_2$ films as a function of temperature (by prism coupling) have also been completed.

Another part of this thesis work (Paper **III**) deals with Guided Mode Resonance Filters (GMRFs) [13, 14] buried by ALD-grown $TiO_2$. Burying surface-relief structures by $TiO_2$ transforms them into volume-type elements with a nearly flat top surface. These buried structures offer easy cleaning due to their flat-top fidelity. Hence they can be re-used in, e.g., sensing applications without any noticeable damage to the cover layer/structure or any deterioration in the optical response even after cleaning and re-using a number of times. These mechanically robust structures should find wide applicability in resonance-domain diffractive optics [15–18] and in realization of quasi-planar meta-materials [19–21].

The thin $TiO_2$ and $Al_2O_3$ films and the $TiO_2$–$Al_2O_3$ bilayers fabricated by ALD are characterized by Variable Angle Spectroscopic Ellipsometry (VASE), Atomic Force Microscopy (AFM), X-ray Diffractrometry (XRD), and Scanning Electron Microcopy (SEM). The GMRFs are designed by the Fourier Modal Method (FMM), fabricated by Electron Beam Lithography (EBL) and Reactive Ion Etching (RIE), buried by ALD, and characterized by SEM and spectroscopic measurements.

## 1.1 OUTLINE

The thesis consists of six chapters, which are outlined as follows. The present chapter provided a general introduction to the studied field, the specific problems addressed, the objectives of the work, and the major breakthroughs achieved. Chapter 2 illustrates the theoretical background of the theory of thin films, as well as their design, fabrication, and analysis methods. Chapter 3 explains the theory and concept of diffraction gratings, and in particular the main design and fabrication methods of GMRFs. Chapter 4 describes the main experimental techniques used to fabricate and characterize thins films and optical nanostructures. Chapter 5 highlights the main results for the thin films and buried grating structures. Finally, conclusions on major breakthroughs achieved for thin films and GMRFs are presented in Chapter 6, along with an overview of foreseeable future work.

# 2 Optics of thin films

Thin metallic, dielectric, and semiconductor films are widely exploited in optical coatings either in the form of a single layer or in layered stacks consisting of materials with different properties. Apart from their use in reflecting optical telescopes, the first famous utilization of thin metal films dates back to 1899 when the Fabry-Perot interferometer was developed, which required high-reflectance mirrors to achieve good resolution in spectroscopy, thus enabling great advancements in this research area. The use of dielectric thin films in coating optical lenses was greatly promoted by Lord Rayleigh and Fraunhofer. The use of coated lenses found immense applications in optical imaging devices, such as microscopes, binoculars, telescopes, and cameras. The use of dielectric thin films also found use in dielectric mirrors, optical filters, selective absorbers, etc.

The focus on the use of optical thin films has extended quite radically from traditional optical components to newly emerging devices. Nowadays, thin films have a wide variety of applications in many domains of optics and photonics. They are used as highly reflective coatings in laser cavities, in material systems for integrated photonics structures, in anti-reflection coatings for solar cells, and as barrier layer coatings to impede permeation and protect environmentally sensitive devices in varying atmospheric conditions, to mention a few [22, 23].

When light in the form of electromagnetic waves is incident on a single film or a stack of thin films in a layered combination (stratified medium) from the outside, it reflects and refracts at all interfaces. The optical response is then a superposition of all multiply reflected and transmitted fields. A thin film (or film stack) can also act as a waveguide that supports propagating modes when the refractive index of the film is higher than those of the surrounding substrate and superstrate media. In addition to these bound modes, each of which propagates along the waveguide without a change in spatial profile, light waves can radiate from the film into the substrate or into the superstrate. The last two types of modes can be termed as radiation modes. These possible modes are all solutions to the Maxwell's equations that also meet the electromagnetic boundary conditions at the film-substrate and film-superstrate interfaces. They can also be explained by Snell's law of refraction and the total internal reflection phenomenon [24].

In general, considering external illumination of a film or film stack, a part $R$ of the incident energy is reflected from the entrance surface, a part $T$ is transmitted through the exit surface, and a part $A$ is lost because of absorption inside the object. Furthermore, a part $S$ is effectively lost because of scattering from imperfections such as surface roughness, density variations due to surface and internal structure porosity, cracks, pinholes, impurities, etc. Then energy conservation gives the relation

$$R + T + A + S = 1. \tag{2.1}$$

The exact computation of the coefficients $R$, $T$, and $A$ for any film or stratified medium is discussed in detail in all standard optics textbooks. However, theoretical estimation of the scattered part is a far more difficult task.

## 2.1 THIN-FILM DEPOSITION METHODS

The deposition methods of thin films date back to the latter half of $19^{th}$ century when Grove, in 1852, observed that metal deposits from a glowing cathode discharge. In 1859, Faraday produced evaporated thin films from exploding fuse-like metal wires in an inert atmosphere. Two of the most famous and important methods of thin film deposition in existence until today are sputtering and vacuum evaporation, which fall into the category of Physical Vapor Deposition (PVD). These methods evolved and gained popularity through various device and process development advances. The main difference between these two deposition methods is that in the former method the atoms are removed from the source material by thermal process, whereas in the latter method the atoms are knocked out of the source material by means of energetic gaseous ions. Although these deposition methods have been in use for decades, they involve some compromises on the quality of thin films. Defects such as film thickness non-uniformity, impurities, pinhole defects, cracks, density variations, films adhesion problems, porosity, etc., remain still major issues [22].

In the Chemical Vapor Deposition (CVD) method [25], a direct chemical reaction between a volatile compound of some material with suitable gases/gaseous reactants atomistically deposits a desired nonvolatile thin film on a heated substrate surface. The CVD method was adopted fast because of its immense advantages in deposition of a variety of metal coatings and thin films, semiconductor coatings, and other compounds either in amorphous or crystalline form. CVD allows to control the stoichiometry of the film, together with the privileges of relatively low-cost process and equipment. However, with the passage of time, many variants of CVD processing along with hybrid processing employing physical and chemical vapor depositions were also developed [26,27]. The selection of the most suitable method for thin film deposition among the many presently available variants is based on the desired film quality and intended applications/market [28].

## 2.2 ATOMIC LAYER DEPOSITION (ALD)

One of the most recent additions to the selection of thin-film deposition techniques is Atomic Layer Deposition (ALD), developed by Tuomo Suntola in 1979 in Finland [29]. ALD is an advanced form of CVD processing and superior over CVD and other deposition techniques in many ways. In ALD, two gaseous precursors are pulsed to the substrate surface periodically (e.g., in alternating precursor cycles), resulting in precise thickness control at atomic scale. It facilitates uniform conformal growth of pinhole and defect free thin films, starting from few-nanometer-thick monolayers up to the desired thickness [30], and it is therefore used extensively in nanoscale device fabrication. ALD allows material deposition in a broad range of temperatures, typically from $\sim 50^{\circ}C$ to $\sim 500^{\circ}C$ [31]. In addition, the development of roll-to-roll ALD enables its use at industrial scale [32]. A detailed overview of the ALD technique is presented in Chapter 4.

Some of the most important thin-film materials deposited by ALD with excellent optical, thermal, and mechanical characteristics are $TiO_2$ and $Al_2O_3$ [33]. Since, in this thesis, we deal with such films and their bilayer combinations, a brief introduction to their properties (based on the achieved results) is given in the following sections.

### 2.2.1 $TiO_2$ thin films

Amorphous ALD titanium dioxide ($TiO_2$) thin films are known for their stable and favorable properties such as: high refractive indices, low absorption losses, large bandgaps, stability at high temperatures, excellent transparency in VIS and IR spectral regions required in many optical sensor devices, photoactivity (hydrophilicity), and the photocatalytic characteristics. One important aspect of ALD deposited $TiO_2$ films is the adsorption of hydrogen containing species or oxygen vacancies formed during the growth process that contribute to the changes in the refractive index of the films later during the operational stages. In fact, such films undergo environmental effects. Temperature, humidity, and moisture effects can also be accompanied by a bandgap change of optical dielectric films due to adsorption of hydrogenated species or formation of oxygen vacancies at interstitial positions. One such change (positive or negative) is represented by the thermo-optic coefficient (TOC) $\mathrm{d}n/\mathrm{d}T$, which measures the change in the material's refractive index as a function of temperature. It is further known that the thermo-optical properties of thin films in various optical sensors based on stacked layer structures are thickness dependent. ALD-$TiO_2$ thin films of thicknesses $< 150$ nm exhibit a decrease in refractive index with an increase in temperature (negative TOCs), whereas thicker films ($> 150$ nm) exhibit positive TOCs. The reason for the decrease in refractive index or negative TOC and density changes is the evaporation of hydrogenated ($H_2O$, OH etc.) species situated at the near surface region of thin ALD-$TiO_2$ films thus forming a widespread depletion region (porosity region).

It has been demonstrated that higher-thickness ALD-$TiO_2$ thin films (carrying positive TOCs) can be used in athermal optical device configurations (e.g., in replicated guided mode resonance filters/gratings), in thermal sensors where change in optical constants with temperature has a significant effect, as protective and/or diffusion barrier layers, as optical coatings in smart device structures, and in many other applications [4, 34].

### 2.2.2 $Al_2O_3$ thin films

Alumina ($Al_2O_3$) or aluminum oxide is typically formed by the aluminum metal. Its naturally occurring mineral forms include: Corundum ($Al_2O_3$), Diaspore ($Al_2O_3$.$H_2O$), Gibbsite ($Al_2O_3.3H_2O$), and Bauxite. It also exists in the form of Boehmite, Bayerite, and Nordstrandite in nature. The naturally occurring alumina has hexagonal unit cell structure but it also has octahedral sites and also exists in liquid structure form. The presence of strong oxygen chemical bonding in its structural forms is the base of its excellent optical, thermal, electrical, mechanical, and chemical characteristics.

Atomic layer deposited $Al_2O_3$ thin films carry favorable properties like chemical inertness, insolubility in most chemical reagents, thermal stability at high temperatures, high refractive index, positive thermo-optic constants, low loss and high transparency from near ultraviolet (UV) to near IR spectral regions. These excellent features of ALD-$Al_2O_3$ thin films pave the way for their use in a wide variety of applications. These films are used especially in integrated optics to realize low-loss optical waveguides, integrated optical waveguide devices for biological and chemical sensors, waveguides for the telecommunication window around 1.5 $\mu$m, etc.

In addition to the above-mentioned properties and usages, the chemical inertness and excellent stability properties of ALD-$Al_2O_3$ thin films make them capable

of resisting the diffusion and permeation of any material inside the film. Hence these films can act as protective and/or diffusion barrier layers, and find plenty of applications in electronics, optics and photonics [34,35].

### 2.2.3 $TiO_2$–$Al_2O_3$ bilayers

As both ALD-$TiO_2$ and $Al_2O_3$ thin films carry excellent characteristics, their combination enhances their respective barrier and other capabilities. It has been shown that when an ALD-$Al_2O_3$ thin film is deposited onto an ALD-$TiO_2$ deposited stainless steel substrate, the $Al_2O_3/TiO_2$ bilayer combination enhances the substrate's protective ability against corrosion by strongly reducing corrosion current density. Bilayer and multilayer configurations of ALD-$Al_2O_3$–$TiO_2$ thin films show better corrosion protection of the stainless steel substrate than single layers of either of these films, especially ALD-$TiO_2$ films [36].

As stated earlier, the refractive index of thin ALD-$TiO_2$ films decreases with increasing temperature and consequently its $dn/dT$ value is negative. This is because of the decrease in the film's density due to existence of pores that are filled with hydrogenated species on the film's surface and vaporize upon increasing temperature. The combination of ALD-$Al_2O_3$ and $TiO_2$ thin films as a bilayer contributes to filling pores/holes that exist near the surface of $TiO_2$ thin films. The refractive index of ALD-$Al_2O_3$ thin films shows an increase at higher temperatures, giving positive $dn/dT$ values [12]. This, together with the protective nature of $Al_2O_3$, leads to positive TOC also for thin bilayers.

The use of bilayers is also believed to improve the performance of GMRFs by stabilization of the spectral shifts that are induced due to thermal changes. Such stable nanophotonic devices have extensive scope in sensor industry [34,35].

## 2.3 THIN-FILM CHARACTERIZATION METHODS

There exist several methods for optical and structural characterization of thin films. Scanning electron microscopy and atomic force microscopy techniques are two of several structural characterization methods, which were in use also in the present work. Spectroscopic ellipsometry [37] is one of the several techniques for optical and thermo-optical characterization of thin films. This technique was used for characterization of both single-layer films and bilayer structures, and a brief description of it follows.

### 2.3.1 Spectroscopic ellipsometry

Spectroscopic ellipsometry is an optical characterization technique that detects the changes introduced in the polarized incident light beam as a result of reflection or transmission from the sample's surface. The refractive index $n$, the extinction coefficient $k$, and the thickness $T$ are extracted by fitting the measured ellipsometric data with a model for the layered structure [38]. Interpretation of the data and the retrieval of the complex refractive index of a material are, in the simplest case, based on Fresnel's reflection/transmission equations for polarized light as discussed in more detail in Chapter 4.

A comparison between the deposition quality of $TiO_2$ thin films grown by Atomic Layer Deposition (ALD) and Electron Beam Evaporation (EBE) methods is shown in Fig. 2.1. The superior quality of the ALD-grown film is evident.

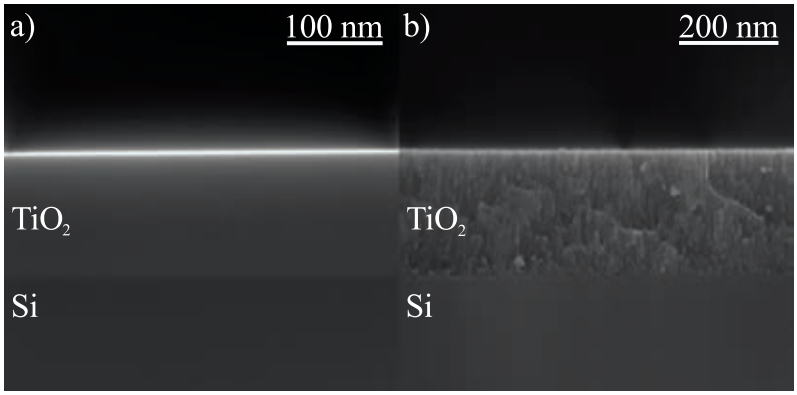


**Figure 2.1:** Cross-sectional SEM images showing the deposition quality of $\sim$ 300 nm $TiO_2$ thin films grown by (a) atomic layer deposition and (b) electron beam evaporation methods on Si substrates [34].

# 3 Diffraction and gratings

## 3.1 DIFFRACTION GRATINGS

It has been well established by both theory and experiments that light has dual nature, i.e., it possesses both wave and particle characteristics. The wave characteristics are supported by classical optics, whereas the particle characteristics are supported by quantum optics [39, 40]. Diffractive optics is based on the wave nature of light, manifested by the classical phenomena of diffraction [17]. Diffractive optical elements (DOEs) are permittivity-modulated micro structures, which can be realized as micro-relief profiles. These profiles may be globally periodic surface-relief or index-modulation structures, or they may be only locally periodic, such as diffractive lenses [41–44]. Although some features of DOEs can be described by geometrical optics, their complete characterization requires wave optics [45–47].

A diffraction grating, or simply a grating, consists of a series of reflecting or transmitting elements, which are separated by a distance (i.e., period) usually greater than, comparable to or less than the interacting light wavelength [48]. The main fundamental physical characteristic of the grating element is the spatial modulation of the (possibly complex) refractive index [49]. The light diffraction from a grating structure with period $d$ is generally represented by the grating equation

$$n_2 \sin\theta_m = n_1 \sin\theta_i + m\lambda/d, \tag{3.1}$$

where $n_1$ and $n_2$ are the refractive indices of the incident and output media, respectively, $\theta_i$ and $\theta_m$ are the incident and diffracted light wave angles with respect to the grating normal, $m$ represents the index of the diffraction order, and $\lambda$ is the vacuum wavelength (for reflection gratings $n_2 = n_1$).

Depending on the application, the grating period $d$ can vary from sub-wavelength scale to tens of wavelengths. If $d$ is at least several times larger than the wavelength of light, one observes a number of propagating diffraction orders. This number reduces with the decrease in $d$ but also depends on the angle of incidence of the illuminating light beam and the refractive indices of the surrounding media, as indicated by Eq. (3.1). When the number of propagating diffraction orders is small e.g., generally in case of reflection gratings (where $\lambda/d \sim 1$), one frequently talks about the resonance domain [49–51]. Since in this domain anomalous effects, including Rayleigh, Wood, guided-wave, and plasmon-excitation resonances are commonplace and play a prominent role. With proper design of the grating structure, for example the first diffraction order can be made dominant [52, 53]. Finally, when the grating period is below the wavelength of the incident light, one speaks of sub-wavelength gratings. For sufficiently small values of $d$, only the zeroth diffraction orders (transmitted/reflected) propagate and all higher orders are evanescent. If $d \ll \lambda$, the physical refractive-index distribution within the grating can often be approximated by an (averaged) effective refractive index, which depends on the state of polarization of incident light [54]. Then the grating layer acts much as a (generally birefringent) spatially uniform thin film.

It should be noted that the effective-index model is not valid for all gratings that support only the zeroth reflected and transmitted orders. This is because effective-

medium theories do not account for evanescent fields or guided/plasmonic modes propagating along the direction of the modulated grating surface. If $d \approx \lambda$, resonant coupling into evanescent fields can be strong. The guided mode resonance filters discussed in this work are examples of such gratings. While these structures may reflect and transmit only the zeroth orders, resonant coupling of light into (leaky) waveguide modes causes anomalous transmission/reflectance properties that are not accessible by effective-medium theories.

The origin of the resonant nature of diffraction gratings came into existence by Wood in 1902. He observed sharp variations in the reflection spectra of metallic gratings, manifested as bright and dark bands for TM-polarized light, which he called anomalies [55]. Lord Rayleigh in 1907 presented a theoretical explanation for these anomalies as the appearance of a particular spectral order at grazing incidence. These spectral positions of the so-called Rayleigh anomalies follow directly from the grating equation. However, not all anomalies observed by Wood can be explained in this way. Rapid spectral modulations also occur near (but not exactly at) the Rayleigh wavelengths, and these are associated with the excitation of surface plasmon waves that propagate along the grating surface [51]. While such anomalies occur only in TM polarization for metallic surface-relief gratings, anomalies of similar nature can (under certain circumstances) be observed in dielectric gratings for any state of polarization. These are associated with the excitation of guided waves that propagate within and near the modulated region of the gratings [56, 57]. This is indeed the operation principle of guided mode resonance filters to be described in more detail below.

In order to analyze resonance-domain gratings computationally, one needs to employ numerical methods to solve Maxwell's equations based on rigorous diffraction theory. This can be done either in the space time-domain or in the spatial-frequency domain [58]. The most common methods employed are the Finite Difference Time Domain (FDTD) method (for time-domain analysis of Maxwell's equations) [59] and Finite Element Method (FEM) (a frequency-domain method) [60]. A method, namely the Fourier Modal Method (FMM) (a spatial frequency-domain method), which is considered the most efficient and accurate electromagnetic analysis frameworks in optics and photonics for most purposes [61], has been is used in the present work.

## 3.2 GUIDED MODE RESONANCE FILTERS (GMRFs)

In a variety of optoelectronic and photonic devices based on gratings, the ability to withstand extreme conditions (high input energy, varying temperature, pressure, humidity etc.) without a significant change in functionality is an important issue. High operational stability is important to ensure consistent performance of optical devices such as Distributed Feedback (DFB) lasers [62], Grating Surface Emitters (GSEs) and GSE arrays [63, 64], and many others [1]. In many applications, guided mode resonance filters (GMRFs) are also required to retain high performance in harsh environments. This is particularly true in many sensor applications, and improving the environmental resistance of GMRFs is one of the central goals of the present work.

### 3.2.1 Background, basic operation and applications

Guided mode resonance filters [65–67] can be realized in many structural forms (see Fig. 3.1 for some simple examples), but all of them are based on the same basic concept. Incident light that arrives externally at such a structure can, under suitable resonant conditions, be coupled into a guided mode of the waveguide. However, because of the periodic modulation, the waveguide is leaky and therefore light is eventually coupled out of it in the form of radiation modes. The result is a sharp spectral response, which occurs in the form of a narrow reflection peak at particular wavelength that depends on the incident angle, the refractive-index, and the geometrical parameters of the grating structure. The GMRFs are sensitive to the polarization states of incident light waves, with different resonance positions in Transverse Electric (TE: electric field vector is perpendicular to plane of incidence) and in Transverse Magnetic (TM: electric field vector is in the plane of incidence) polarizations.

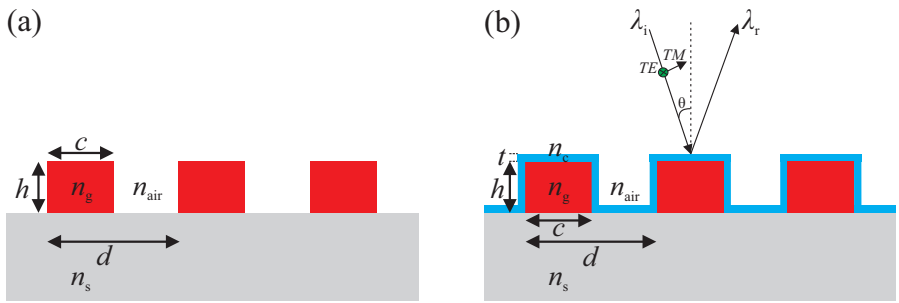


**Figure 3.1:** Cross-sectional structures of some simple GMRFs. (a) Binary index-modulated structure. (b) Thin-film waveguide modulated by a binary surface-relief profile.

The sharpness (narrow/broad) and form (symmetric/asymmetric) of the spectral peaks depend on the design parameters of the grating structure, which are limited and influenced by the fabrication procedure as well. The overall reflectivity of GMRFs is generally affected by the angle of incidence, the cover layer material, other associated design parameters, the structural deviations due to fabrication, and also by temperature variations during structural characterizations, especially in the case of polymeric structures [68–70]. The overall reflectivity also depends on the shape and size of the illuminating fields, as one can readily appreciate by decomposing the incident field into an angular spectrum of plane waves. Since the GMRF response depends on the angle of incidence, not all plane waves included in a finite incident field satisfy the guided-mode resonance condition exactly. Filters can be made non-polarizing and temperature-independent (athermal) using suitable design parameters and choice of cover layer material [71,72].

### 3.2.2 Design by the Fourier Modal Method (FMM)

A GMRF should produce the reflection peak of a certain width at a specified spectral position depending on the intended application. As already indicated, these features

depend strongly on the structure of the GMRF and the refractive indices of the substrate and superstrate media, as well as on the angle of incidence. The design goal is then to choose the grating parameters to meet these goals. For example, in the case of Fig. 3.1(b), the structural parameters to be optimized in design are the grating period $d$, the thickness $t$ of the waveguide, the groove depth $h$, and the fill factor parameter $c$, provided that the refractive indices $n_s$, $n_g$ and $n_c$ are fixed.

In this work computational parametric optimization is used and the grating response for each parametric configuration is evaluated by the Fourier Modal Method (FMM) described in detail in Ref. [61]. Briefly, in FMM, Rayleigh (plane-wave) field expansions are used outside the modulated region of the grating, whereas pseudoperiodic Bloch-mode field expansions are used inside the grating. The Bloch modes are solved numerically from eigenvalue equations that follow from Maxwell's equations. Then the field expansions inside and outside the modulated region are matched using the electromagnetic boundary conditions. This procedure leads to the complex amplitudes of the propagating and evanescent orders outside that grating, and it also gives the weights of the modes inside the grating. From this information, the electromagnetic field in the entire space can be obtained uniquely.

## 3.3 RATIONALE OF ALD-$TiO_2$ BURIED GMRFs

There is an immediate, growing need to develop cost-effective and reliable biomolecular/chemical sensor technologies. Most biosensor technologies currently available are based on fluorescent or absorption labeling to account for a specific biomolecular reaction. In order to develop low-cost and highly efficient sensors with quick response and accurate output, there is an increasing demand for sensor technologies without the use of labeling. These sensor technologies must cover a wide range of molecules to be screened selectively with a least assay development using available antibody-antigen, nucleic acids, and other highly selective bio-materials broadly applicable in biomedicine based on photonic resonance concept. The nature of leaky excited modes depends on both the surface pattern and the underlying structure. Leaky modes, known as surface plasmons, can be excited on purely surface-modulated metallic gratings. They can also be generated on flat metal surfaces coved with periodically modulated dielectric layers. In all dielectric- and semi conductor-based periodic structures, the excitation of leaky modes is based on the guided-mode resonance effect, which requires a sufficient effective-index contrast between the modulated (volume) region and the surrounding media.

Previously, a number of optical sensors for bio- and chemical detection have been reported, including label-free sensor technologies such as Surface Plasmon Resonance (SPR) sensors [73], MEMS based sensors [74], nano-sensors (particles, wires, belts, rods) [75], resonant mirrors [76], Bragg grating sensors [77], waveguide sensors [78,79], waveguide interferometric sensors [80], ellipsometry [81] and grating coupler sensors [82]. The SPR sensors are analogous in features and operation to the GMRF sensors, although different in concept and function. Surface Plasmon (SP) refers to the oscillation of an electromagnetic field charge-density at an interface between a conductor and a dielectric (e.g., gold/glass interface). The SP mode is excited at resonance by incident TM-polarized light only, and results in an absorption minimum at a specific wavelength band. The angular and spectral sensitivities are not very high for SPR sensors compared with other sensors, which have a relatively large FWHM. But, a SPR sensor can detect bio-molecules using only a

single polarization (TM) state and the corresponding changes in the refractive index and bio-layer attachments cannot be resolved simultaneously in one measurement, which limits their use in portable diagnostic applications where thermal variations occur, in comparison to GMRF sensors [83,84].

We propose label-free [85] GMRF-based sensors exploiting tuning on variation in resonance structure parameters specifically, including cover layer thickness and refractive indices. In the proposed approach, the GMRF sensor is based on the high parametric sensitivity that is inherent to the fundamental resonance effect for both TE- and TM-polarization states. It is based on the same concept as if an attaching bio-molecular/chemical layer, which changes the parameters (mostly thicknesses and refractive indices in our case) of the ordinary surface-relief resonant element and leads to the corresponding sharp spectral wavelength variations. In the proposed GMRF sensor, a target analyte interacting is placed on a dielectric cover layer (which fully buries the surface-relief grating profile), can thus be identified without additional processing for any polarization state.

The research work focuses on the development of compact, high performance, buried and nearly flat-top GMRFs based sensors. The sensor is based on a periodic dielectric waveguide of the type illustrated in Fig. 3.2. The starting point is a binary high-aspect-ratio GMRF made of a high-index material on a lower-index substrate. Then ALD-coating is applied until the binary structure is effectively buried in a lower-index material, resulting in a nearly flat top surface. The design of such buried GMRFs is discussed in detail in Chapter 5.

The input light is efficiently reflected in a narrow spectral band whose central wavelength is highly sensitive to chemical reactions occurring at the sensor surface. The spectral resonance wavelength depends on the periodicity and refractive indices of the structure and surrounding media. Interaction of a target analyte with a dielectric cover layer on the sensor surface results in measurable spectral/angular shifts that directly identify the binding event without involvement of a foreign tag (it implies that the detection methods do not require the use of chemical indicators for read-out, such as fluorescent, luminescent or radioactive materials). A bio-/chemical-selective layer is incorporated on the sensor surface that is buried with dielectric cover layer to give a specific spectral effect during operation. Such sensors are responsive to thickness changes from the nanoscale to several $\mu$m, thus comparable to other sensors and planar waveguide configurations. The proposed plan motivates to develop sensor technology that can be used to detect binding events at the molecular level as well as for analytes with micron-scale dimensions.

When a broadband light source illuminates buried GMRF sensors, a specific wavelength of light is reflected at a particular designed angle encountering a binding interaction of an immobilized dielectric cover layer with an analyte (a bio-/chemical-layer) and corresponding spectral shifts (for both TE/TM-modes) can be easily measured by a spectrophotometer or an ellipsometer. Since the excited resonance is polarization dependent that produces separate resonance peaks for TE- and TM-polarizations. The sensor element covalently bonds a selective detection layer and the sensor is multi-functional (with its known specific spectral shift positions for TE-and TM-polarization states) as only the sensitizing surface layer needs to be detected based on sensor's known polarization states. Such kind of sensors can also be designed and fabricated to yield polarization-independent spectral characteristics by evaluating common geometrical parameters of the GMRFs, simply at the point of intersection of dispersion curves for corresponding TE- and TM-modes. However, the linewidths of the spectral curves (TE/TM) may be different depending on the

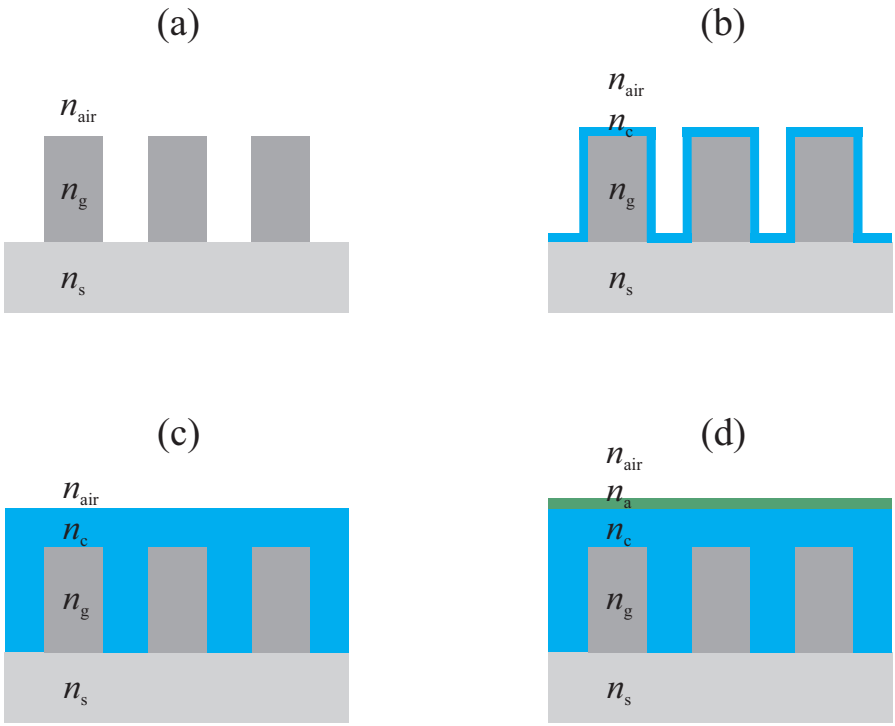


**Figure 3.2:** The concept and fabrication of buried GMRFs. (a) A high-aspect-ratio binary GMRF. (b) The structure coated conformally by a thin ALD film. (c) The structure buried completely by ALD. (d) The ALD buried structure with sensing analyte on top.

effective refractive indices encountered by the light. Buried GMRF based sensors can easily be designed and fabricated to operate in the near-IR wavelength range where most bio-/chemical sensors show minimum absorption.

The goal of this proposed research is to investigate and develop (design, fabrication, and characterization) functional buried and flat-top bio-/chemical GMRF sensors based on GMR effect on an inorganic substrate. The same concept can be extended to polymeric resonant waveguide grating based sensors using optical grade polymer materials such as Polycarbonate (PC), Cyclic Olefin Copolymer (COP) and Ormocomp (OC) etc. [86, 87]. The fabricated sensors can be helpful for the diagnostic purposes as reusable sensors because of an ease to clean the sensing surface after detection measurements. Such sensor technology may be broadly applicable to medical diagnostics, drug discovery and development, industrial process control and environmental monitoring, and plenty of other exciting nanophotonics applications [88].

# 4 Fabrication and characterization methods

## 4.1 ELECTRON BEAM LITHOGRAPHY (EBL)

Lithography is a process of creating, printing, or transferring patterns on some material, with its roots deep in history [89,90]. Today, there exists a variety of lithographic approaches such as electron beam, nanoimprint, X-ray, ion-beam, dip-pen, and extreme ultra-violet (EUV) methods [91] suitable for micro- and nano-patterning. Electron beam lithography (shortly e-beam lithography or EBL) is a versatile technique to directly write designed patterns on an electron-sensitive resist, with the capability of producing features down to a few tens of nanometers in size. A schematic of basic EBL optics and process is illustrated in Fig. 4.1.

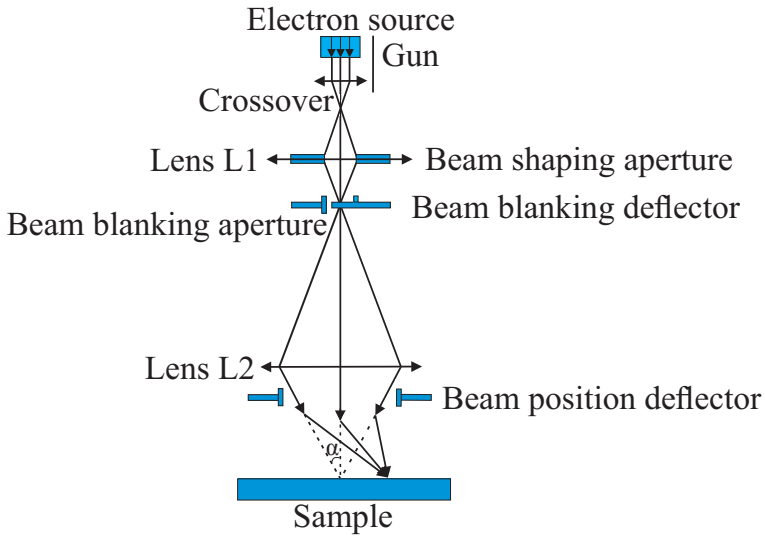


**Figure 4.1:** Schematic of basic EBL optics and process (Reproduced with kind permission Ref. [45]).

The idea of e-beam lithography was proposed by Buck and Shoulders in 1958 and two years later, this idea was demonstrated in practice by Möllenstedt and Speidel [92]. The development and application of the EBL technique to the fabrication of micro- and nano-optical elements in diffractive optics was largely pioneered by Ernst-Bernhard Kley *et al*., in Jena, Germany over the past few decades [93,94].

In EBL, the desired patterns are drawn when incident radiation (a focused electron beam) under high accelerating voltage (usually in kV range) interacts with the resist and produces a physical alteration in it. As a result, either the exposed part of the resist (positive resist) or the unexposed part (negative resist) is removed during

the development process. The patterned resist acts as a binary mask for further processing. The desired pattern to be written is drawn on a compatible software. This data is converted into a format recognized by the e-beam writer. The e-beam then scans the resist surface by means of magnetic field according to the electronic data received and starts the writing process.

The resolution of EBL is not limited by the electron-optical system itself; rather it depends on the resist resolution, electronic interactions within the resist by scattering processes, and other subsequent fabrication process steps [91]. Patterns with features finer than 5 nm can be drawn using commercially available resists when the electron beam is accelerated at around 100 kV. However, EBL is a time-consuming process since patterns are drawn serially and the writing time is directly dependent on the complexity of the structure. Hence, EBL is best suited for writing structures in low volumes, or in patterning masks that are subsequently used to make replicas in large numbers by optical lithographic or nanoimprint techniques [95–97]. The EBL machine used for patterning the optical nano-structures in this work was EBPG5000+HR manufactured by Vistec [98].

## 4.2 ATOMIC LAYER DEPOSITION (ALD)

In the beginning, Atomic Layer Deposition (ALD) was also known as Atomic Layer Chemical Vapor Deposition (AL-CVD) or Atomic Layer Epitaxy (ALE) that was invented by Tuomo Suntola in 70's in Finland. It was mainly used for the deposition of uniform thin films over wide-range areas of display devices. In early days, AL-CVD/ALE/ALD was mainly used for the production of thin-film electroluminescent display devices. The first successful demonstration that introduced the ALE or ALD technique to the scientific world was the ALD-coated electroluminescent flat panel displays installed at Helsinki airport during 1983–1998. Further developments and modifications in the ALD device design and improvements in the process parameters led to the atomic-level thickness control of thin-film deposition for the reduced device dimensions [34, 99–102]. Commercial availability of ALD reactors accelerated the use of ALD in different domains of industry [29, 34, 103, 104].

Today, the ALD technique allows the manufacture of nearly pinhole-defect-free films with precise atomic-level thickness control, self-controlled alternating surface reactions, and wide-area uniformity. Growth of high quality thin films at temperatures as low as 50°C and also at high temperatures (up to 500°C) [31], excellent conformality over corrugated or zigzag surface profiles, and large batch processing capabilities are a few hallmarks of its versatile characteristics. The basic operation of ALD lies in the self-limiting chemical reactions of alternating precursor molecules on the substrate's surface at specific temperature, which initializes these surface reactions. At first, precursor "A" molecules are pulsed to the ALD chamber, which are adsorbed/chemisorbed on the substrate surface, followed by purging with inert gas ($N_2$) that removes excess precursor molecules or any other by-products. Then precursor "B" molecules enter the ALD chamber and react with precursor "A" molecules, are chemisorbed on substrate surface and make binary compound(s) followed by purging with inert gas to remove extra precursor "B" molecules and/or by-products. In this way one ALD cycle completes and many of these ABAB cycles are needed to form a uniform and high quality film according to the requirements. The growth rate is often expressed as an amount of material deposited per reaction cycle. This inherent nature of the ALD method opens possibilities for deposition of a

variety of precursor materials from metals to oxides, nitrides, phosphides, chlorides, sulphides, and hydroids on variety of substrates, e.g., silicon, silica, polymers, and in fact on any kind of feasible substrate materials [34].

Owing to its excellent merits, ALD covers vast application regimes in optics (integrated optics, diffraction gratings, guided mode resonance optical filters, 3D photonic crystals, etc.), in electronics (e.g., gate oxides, diffusion barrier coatings, multilayered trench capacitors), in nanodevices (e.g., nanomaterials, nanolaminates, nanoparticles, nanotubes, nanodots, etc.), in display devices (e.g., OLEDs, protective layers, plasma displays), in the energy sector (e.g., silicon solar cells, fuel cells) and various other fields such as bio/gas sensing, food packaging materials, permeation barriers, jewelry, and optical telecommunication components [2,34,99–102,105–108].

A schematic of the basic ALD process is illustrated in Fig. 4.2.

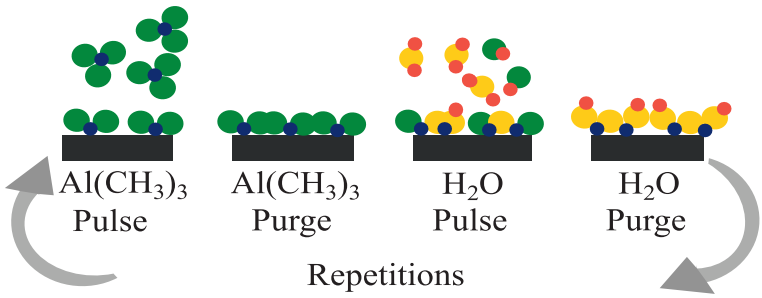


**Figure 4.2:** Schematic of the basic ALD process illustrating the deposition of $Al_2O_3$ film using trimethylaluminum ($Al(CH_3)_3$) and water ($H_2O$) as precursors (Reproduced with kind permission by Beneq [31]).

The commonly used precursors for the deposition of $TiO_2$ and $Al_2O_3$ thin films by ALD are titanium tetrachloride ($TiCl_4$) and water ($H_2O$), and trimethylaluminum ($Al(CH_3)_3$) and water ($H_2O$), respectively [109]. Also, atomic oxygen or ozone replaces water as a precursor material depending on the application. $TiO_2$ and $Al_2O_3$ deposition occurs as a result of the following chemical reactions during CVD process [110,111]:

$$TiCl_4(g) + 2H_2O(g) \rightarrow TiO_2(s) + 4HCl(g)(CVD), \tag{4.1}$$

$$2Al(CH_3)_3(g) + 3H_2O(g) \rightarrow Al_2O_3(s) + 6CH_4(g)(CVD). \tag{4.2}$$

Whereas, in the generally accepted ALD-$TiO_2$ growth mechanism, $TiCl_4$ reacts with the adjacent surface OH (H-bonded OH) groups, releasing hydrochloric acid (HCl) in the first half reaction (ALD A) [112]:

$$n(-OH)(s) + TiCl_4(g) \rightarrow (-O-)_nTiCl_4 - n(s) + nHCl(g), \tag{4.3}$$

where (s) and (g) denote the surface and gaseous phase, respectively. In the second half reaction (ALD B), the adsorbed chlorotitanium reacts with water, releasing HCl again and generating OH groups for the next reaction cycle.

$$(-O-)_nTiCl_{4-n}(s) + (4-n)H_2O(g) \rightarrow (-O-)_nTi(OH)_{4-n}(s) + (4-n)HCl(g). \tag{4.4}$$

Similarly, the reaction cycles of ALD-$Al_2O_3$ growth proceed as follows [113]:

$$Al-OH^*(s) + Al(CH_3)_3(g) \rightarrow Al-O-Al(CH_3)_2{}^*(s) + CH_4(g)(\text{ALD A}), \quad (4.5)$$

$$Al-O-Al(CH_3)_2{}^*(s) + 2H_2O(s) \rightarrow Al-O-Al(OH_2)^*(s) + 2CH_4(g)(\text{ALD B}). \quad (4.6)$$

The $TiO_2$ and $Al_2O_3$ films deposited at 120°C are amorphous in nature but microcrystalline films can also be grown by ALD at higher deposition temperatures. ALD offers many practical advantages over its counterparts in terms of atomic level thickness control, uniform coverage, excellent conformality, pin-hole free films, large area uniformity, etc. ALD, because of its unique thin film deposition characteristics, can deposit a wide variety of metal oxide materials based on the application point of view. In Papers **I** and **II**, the $TiO_2$ and $Al_2O_3$ thin films (also bilayers) were deposited on 2-inch silicon wafers (with 2 nm native oxide layer) using $TiCl_4/H_2O$, and $Al(CH_3)_3/H_2O$ precursors, respectively, at 120°C. The growth rates for the $TiO_2$ and $Al_2O_3$ thin films were 0.065 nm and 0.12 nm per cycle, respectively. The $TiO_2$ thin films were deposited on silica gratings using the same precursors and deposition temperature mentioned above at a growth rate of 0.07 nm per cycle in Paper **III**. The fabrication processes are discussed in detail in Papers **I–III**. The ALD machine used for the fabrication of thin films and optical nanostructures in this work was ALD TFS 200-152 by Beneq [114].

## 4.3 SPECTROSCOPIC ELLIPSOMETRY

Ellipsometry is a non-invasive, non-destructive and in-line optical characterization technique based on the measurement of changes in the polarization state of an incident light beam reflected or transmitted from the sample surface [115]. The basic principle of operation of ellipsometry is based on the determination of the phase change in polarized light after reflection/transmission from the sample. The input light is polarized before its interaction with the sample. Ellipsometer is regarded as an instrument that measures this change [34, 116].

An ellipsometer unit consists of a broadband arc lamp, a monochromator, a fiber optic cable, an input unit consisting of a collimator, polarizer, and an alignment detector with mounting, a rotatable sample stage, iris and nosecone head, an output unit that consists of an analyzer and detector, and a computer with WVASE32 software for controlling almost the entire system. The basic operating principle of ellipsometry is that the arc lamp produces and supplies broadband light to the monochromator. The monochromator selects the desired wavelength. The monochromatic light is then coupled into the input unit through a UV/IR fiber optic cable. The monochromatic light after passing through the input unit becomes collimated and polarized. The input unit establishes the desired polarization state of the input light beam. The monochromatic, modulated, collimated, and polarized light beam is then incident on the sample. After reflection/transmission from the sample, the light beam enters the iris and nosecone unit, with adjustable iris that limits the amount of light entering. The light beam then enters the output unit that consists of an analyzer and a detector endcap. The output unit analyzes and measures the change in the polarization state of light beam. The light beam is then converted into an electrical signal by the output unit and the information is available in digital form for further analysis with WVASE32 software [34, 117].

The mathematical description of the ellipsometry theory is based on Fresnel's reflection and transmission equations for polarized light [34,118]. Since electromagnetic plane waves are (the simplest) solutions of Maxwell's equations, there is a direct relation between Fresnel's and Maxwell's equations for the case of polarized light. The ellipsometric measurements are expressed in terms of parameters $\Psi$ and $\Delta$ and their relation with Fresnel reflection coefficients can be expressed by the relation

$$\rho = \frac{r_p}{r_s} = \tan\Psi \exp\left(i\Delta\right), \tag{4.7}$$

where $\rho$ is the ratio of complex Fresnel reflection coefficients. In $r_p$, subscript $p$ stands for p-polarized light (electric field vector is in the plane of incidence), whereas in $r_s$, the subscript $s$ stands for s-polarized light (electric field vector is perpendicular to the plane of incidence). Since $\rho$ is the ratio of two complex reflection coefficients, the ellipsometric measurements are often accurate [34,119,120]. The quantity $\Psi$ represents the magnitude of the ratio $\rho$ of Fresnel reflection coefficients and $\Delta$ represents the phase difference between these coefficients [116]. The Fresnel complex reflection coefficients $r_p$ and $r_s$ can be further presented by the following equations:

$$r_p = \rho_p \exp\left(i\delta_p\right), \tag{4.8}$$

$$r_s = \rho_s \exp\left(i\delta_s\right). \tag{4.9}$$

The desired optical parameters can be extracted by employing Fresnel's reflection equations after measuring $\Psi$ and $\Delta$ values at a specific wavelength [34, 120]. A schematic of illustration of spectroscopic ellipsometer components is shown in Fig. 4.3.

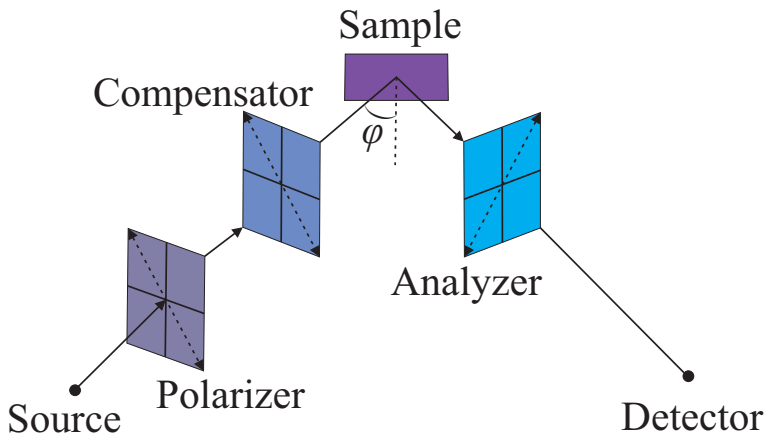


**Figure 4.3:** Schematic of basic illustration of operating principle of spectroscopic ellipsometer (Reproduced with kind permission Ref. [45]).

Variable angle spectroscopic ellipsometer does not measure optical constants, thin film thicknesses, or other optical properties directly. It measures reflected or transmitted intensities in terms of change in the polarization states. The change in the polarization state of a light beam is expressed in terms of $\Psi$ and $\Delta$. Therefore, the modeling of the ellipsometric data based on the relevant theoretical models is

necessary in extracting useful optical information about the sample. First, the ellipsometric data is measured for the desired spectral range and angle of incidence. Second, the optical model that suits best with the available sample structure information is selected. The Fresnel's equations, linked in the selected model, are used for the prediction of the expected data. Third, the comparison between the experimental and model data is established [34, 121]. This procedure is used to extract thickness and optical constants of single layers and individual layers in multilayers as well as other desired optical properties of the sample upon good match between the experimental and model based data curves. There exist several models for the determination of optical constants of thin films that are embedded into WVASE32 software. One among such models is the Cauchy model [34,122–124] that is suitable for the determination of optical constants of transparent and semi-transparent thin films within spectral regions of incognizant absorption.

In the Cauchy model, the refractive index $n$ and the extinction coefficient $k$ can be represented as slowly varying functions of wavelength and exponential absorption tail, respectively, by the following equations:

$$n(\lambda) = A + \frac{B}{\lambda^2} + \frac{C}{\lambda^4} + ...., \tag{4.10}$$

$$k(\lambda) = \alpha \exp\left\{\beta\left[12400\left(\frac{1}{\lambda} - \frac{1}{\gamma}\right)\right]\right\}. \tag{4.11}$$

Here $A$, $B$, and $C$ are the model fitting constants, while the extinction coefficient amplitude $\alpha$, the exponent factor $\beta$, and the band edge $\gamma$ are all fitting parameters of the Cauchy model [34,122].

The Cauchy model provides good fitting quality and useful information about the optical properties of dielectric and semiconductor thin films. It also explains the behavior of $\Psi$ and $\Delta$ curves near the band edge that is approximately in the wavelength range from 375 nm to 410 nm. The inclusion of the exponential absorption tail is useful for the correct explanation of sub-band-gap absorption near the band edge in the case of thin oxide films [34,125].

The spectroscopic ellipsometry technique equipped with variable angles of incidence allows acquiring more information about the sample. Variable angle spectroscopic ellipsometric measurements involve the use of variable angles of incidence and wide spectral range. The variable angles of incidence in spectroscopic ellipsometry can be attributed to acquiring data near the pseudo-Brewster angle for the sample. At pseudo-Brewster angle, the sensitivity of ellipsometric measurements is high when the measured $\Delta$ values are close to 90°. For semiconductors and low refractive index materials, the pseudo-Brewster angle is near 75° and 60°, respectively [34,116]. The variable angle spectroscopic ellipsometer is very popular for research on new materials and processes. Variable angle spectroscopic ellipsometers are commercially available with a wide spectral range from 150 nm to 3300 nm [34, 119] and angles of incidence from almost 15° to 90° with an accuracy of 0.01° [34, 126].

Ellipsometry is not limited to just measuring thin film thicknesses, optical constants, and many other physical quantities. But, it is also used to characterize both thin films and bulk materials from extremely thin to many microns thick samples. Ellipsometry measurement areas include (but are not limited to) the determination of: Alloy ratio, birefringence, cross-polarized reflection or transmission, crystallinity, depth profile of the material, depolarization, doping concentration, growth rate, optical anisotropy, optical constants like refractive index, extinction coefficient,

and/or dielectric constants in UV, VIS and IR spectral ranges; retardance, reflectance and transmittance intensity, surface roughness, surface uniformity of samples, temperature, etc. [34,116,119,121,127]. Thin films and optical nanostructures were characterized by a Variable Angle Spectroscopic Ellipsometer (VASE) with a High-Speed Monochromator System HS-190 by J.A. Woollam [128].

## 4.4 OPTICAL CHARACTERIZATION METHODS

### 4.4.1 Scanning electron microscopy (SEM)

A scanning electron microscope (SEM) is basically used to capture high quality images of an object under consideration. The SEM uses a high energy beam of electrons produced by an electron source, which is first focused by a condenser lens and then again by an objective lens followed by scan coils. After traveling through a number of lenses and apertures, the focused high-energy beam interacts with the sample atoms and as a result of beam-sample interactions, the electrons are released. The knocked-out electrons are known as secondary electrons and these are detected by a scintillation material, which produces flashes of light from the secondary electrons, and the information collected from them is transformed into the image/topology of the surface. These beam-sample interactions can also result in the emission of backscattered electrons, photons, and heat [129–132]. The SEM system used for structural characterization of thin films and optical nanostructures was LEO 1550 Gemini by Zeiss [133].

### 4.4.2 Prism coupling (PC)

A prism coupler is an optical characterization device, with which one can accurately measure the thicknesses, refractive indices, effective indices/birefringence of dielectrics and polymer films, in addition to refractive indices of bulk materials. The prism coupler measurement system consists of a prism, the coupling head, three lasers, a photodetector, temperature controller, and a computer controlled rotary table. The film whose refractive index and thickness to be measured is brought in contact between the coupling head and a prism. The laser light is incident onto the prism base and is totally internally reflected to the photodetector. Since a small air gap exists between the film and the prism, at certain discrete angles set by the rotary table, the photons tunnel through the air gap into the film and support guided optical propagation modes. The rotary table varies the incident angle and locates the modes automatically. The angular location of the first mode determines the refractive index of the film, whereas the angular difference between two modes determines the thickness.

A prism coupler offers several practical advantages over its counterparts, e.g., refractrometers, ellipsometry, and/or spectrophotometry in terms of index measurement accuracy, high resolution, high stability, rapid and error-free characterization, easy index vs. wavelength measurements, index vs. temperature measurements ($dn/dT$), and waveguide losses with wide index measurement range. We utilized Metricon Model 2010/M prism coupler [134] for characterization measurements of amorphous and crystalline ALD-$TiO_2$ thin films.

### 4.4.3 X-ray diffractometry (XRD)

X-ray diffractometry is a process of identification of unique fingerprints of element(s) present in amorphous, crystalline, poly-crystalline, or compound materials. Its principle is based on the detection of diffracted beams, which consist of a large number of scattered and mutually re-inforced rays, from a series of single crystal planes often termed as X-ray diffracted beams [135]. X-ray diffraction measurements were carried out with Advance D8 device by Bruker [136].

### 4.4.4 Atomic force microscopy (AFM)

Atomic Force Microscopy (AFM) is an essential tool to study the surface topographical properties of a wide variety of samples at nanometer scale. It offers 3D surface profile measurements of a sample and its primary modes of imaging surfaces are contact mode, dynamic mode (tapping), non-contact mode (oscillating). In principle, AFM consists of a very small and sharp probe (tip) attached at the apex of a flexible cantilever. A piezoelectric scanner is used to move the sample in three dimensions at a sub-nanometer scale upon applied voltage. The semiconductor diode laser is used to bounce off the beam on to the probe (tip) when it touches or scans the surface of a sample. The small forces between the surface and the probe are recorded via a photodetector in terms of deflections caused by the bending of cantilever to form a line-by-line image of the sample [137–139]. The AFM system used for structural characterization of optical thin films was AFM, MultiMode with High-Speed ScanAsyst-Air Mode by Bruker [140].

# 5 Results

## 5.1 THIN FILMS

In this section, we present the experimental results related to the optical characterization of thin films.

### 5.1.1 Determination of thermo-optic coefficients (TOCs)

The thermo-optic coefficient $dn/dT$ is a measure of the change in material's refractive index with respect to temperature. The TOC of a material can have a negative or a positive value. In the former case, the refractive index of a material decreases with increasing temperature, while in the latter case it increases with temperature. The permeation of foreign molecules, such as water molecules or hydrogenated species, through a material surface is determined by the TOC value of a material. In addition, TOC values are dependent on material thickness. A negative TOC value indicates that the material surface is permeable (i.e., porous) and a positive TOC implies impermeable behavior of the material surface (i.e., non-porous). Most often, refractive index change with temperature correlates well with the density in the case of a homogeneous material, but can differ due to the introduction of residual stresses and change in the material's crystal orientations as a result of temperature change. The response of a bound system to an externally applied entity can be described by the Lorentz–Lorenz relation (also known as Clausius–Mossotti relation and Maxwell's formula). Explicitly, the temperature-dependent refractive index of a material can be expressed in the form [141]

$$\frac{n^2-1}{n^2+2} = \frac{4\pi}{3}\alpha_e \frac{\rho N_A}{m}. \tag{5.1}$$

Here $n = n(\lambda,T)$, $\alpha_e$ is the electronic polarizability ($cm^3$), $\rho$ is the material density ($g/cm^3$), $N_A$ is the Avogadro's number ($6.022\times10^{23}$ electrons/mol), and $m$ is the molecular weight of a $TiO_2$ molecule (79.9 g/mol) and 101.961 g/mol for the $Al_2O_3$ molecule.

### 5.1.2 ALD-$TiO_2$ thin films

In order to validate the surface porosity model of $TiO_2$ films in terms of TOCs, fixed-thickness ($\sim$ 6 nm) $Al_2O_3$ diffusion barrier layers were coated on $TiO_2$ films of different thicknesses ($\sim$ 60 nm, 100–500 nm with 100 nm thickness increment), residing on Si wafers, by ALD. We call this set of $TiO_2$–$Al_2O_3$ films $S_{A(1–6)}$. The wavelength- and temperature-dependent refractive indices of $TiO_2$ and $Al_2O_3$ thin films in bilayers were measured by a variable angle spectroscopic ellipsometer (VASE) for two incident angles ($\phi = 65^\circ$ and $75^\circ$), over a wide wavelength range (380–1800 nm) with a scan step of 20 nm and beam spot size of 3 mm. The bilayer samples were heated on a home-made aluminum heating assembly from room temperature ($\sim 20^\circ$C) up to 150°C with a 10°C increment in temperature (i.e., 0.5°C/min increase in temperature) with an accuracy of $\pm0.1^\circ$C.

In order to extract the accurate optical properties of bilayer films measured by VASE, it is important to develop an optical model, which ensures accurate extraction of optical constants upon perfect fitting of experimental data. In our case, we utilize the Cauchy formula (4.10) to calculate the refractive index data of bilayer films measured as a function of wavelength and temperature. After a number of iterations by using initial values of film thicknesses and the Cauchy parameter values, the regression algorithm converges to a perfect fitting of modeled and experimental data. Thus wavelength- and temperature-dependent optical data can be obtained at any wavelength of interest within the measured wavelength range. In our case, we used 640 nm wavelength value due to the fact that this value is quite close to the operating wavelength of the He–Ne laser used for characterization purposes.

In order to model the temperature-dependent refractive indices of bilayer films, the refractive index values are inserted in the reciprocal of the left hand side of Eq. (5.1) for a temperature range 20–150°C with 10°C increment in temperature at a wavelength of 640 nm for any combination of bilayer thicknesses in any set mentioned above. A least-square fit of the plotted curve to the data points gives an equation in terms of temperature coefficients. The differentiation of the resulting equation from parabolic fit with respect to temperature $T$ gives finally an equation in terms of $\mathrm{d}n/\mathrm{d}T$ and insertion of temperature values determines the TOCs at any desired temperature value in $^{\circ}\mathrm{C}^{-1}$ units. A schematic of near surface region porosity concept of a $TiO_2$ film with a thin $Al_2O_3$ barrier layer on the top is shown in Fig. 5.1.

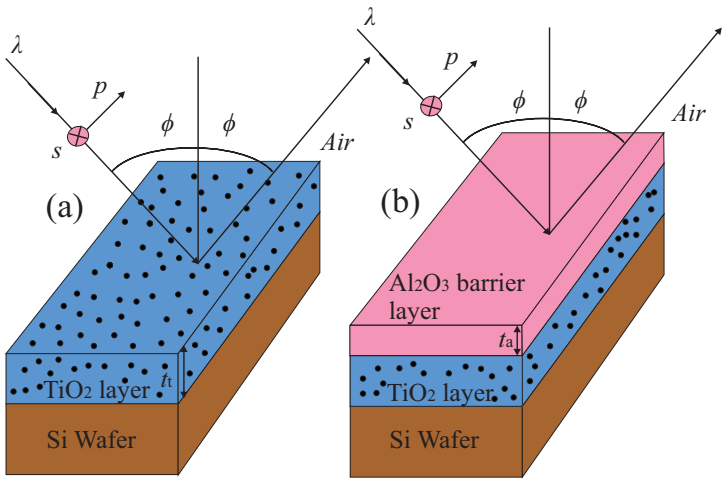


**Figure 5.1:** (a) Schematic diagram of a near surface region porosity concept on $TiO_2$ thin film. (b) $Al_2O_3$ barrier layer model on top of the $TiO_2$ thin film along with the illumination geometry of ellipsometric measurements (Paper **I**).

Similarly, the temperature-dependent density of any film thickness in the bilayer films can de determined on the basis of the measured refractive index by using Lorentz–Lorenz equation (5.1) at a wavelength of 640 nm. The insertion of parametric values and measured index values for each temperature (from 20°C up to 150°C with 10°C increment in temperature) determined at a wavelength of 640 nm, gives data points that yield upon a good parabolic fit. The differentiation of this equation with respect to $T$ leads to a final equation in terms of $\mathrm{d}\rho(T)/\mathrm{d}T$ and insertion of temperature values gives the temperature-dependent density at any desired

temperature value expressed in units $gcm^{-3}{}^{\circ}C^{-1}$.

From the determined TOCs of all films in the bilayers in the sample set $S_{A(1-6)}$, we see from Fig. 5.2(a) that the thinnest $TiO_2$ film ($\sim$ 60 nm) possesses the most negative TOC even in the presence of a $\sim$ 6 nm $Al_2O_3$ impermeable barrier layer. However, the negative TOCs change towards positive for higher $TiO_2$ film thicknesses, as shown in Fig. 5.2(a). The thinnest $TiO_2$ film with the most negative TOC value shows higher evaporation rate of water molecules from the near surface region of the film due to the fact that there might exist some pin-hole defects on the (supposedly impermeable) $Al_2O_3$ barrier layer. The behavior of TOCs for each $TiO_2$ film thickness even with the presence of thin $Al_2O_3$ barrier layers is the same as reported in Ref. [4]. Supposing that an increase in the $Al_2O_3$ barrier layer thickness might be more effective and in order to validate the surface porosity model, we increased the $Al_2O_3$ barrier layer thickness from $\sim$ 6 nm to 36 nm with 6 nm increment on the thinnest $TiO_2$ film ($\sim$ 60 nm). We call this set of $TiO_2$–$Al_2O_3$ films $S_{B(1-6)}$. The results presented in Fig. 5.2(b) show that the increase in $Al_2O_3$ barrier layer thickness from $\sim$ 6 nm to 36 nm does indeed improve the TOC of the underlaying $TiO_2$ films. A 33% overall change in TOCs is determined experimentally with an increase in $Al_2O_3$ barrier layer thickness to $\sim$ 36 nm. This demonstrates well the impeding effect of barrier layer films against the permeation of hydrogenated species at the near surface regions of underlaying $TiO_2$ films. The conclusion is that $Al_2O_3$ barrier layer films that are deposited at low temperatures are amorphous in nature and may have pin-holes and surface defects as a result. $Al_2O_3$ barrier layers deposited at low temperature, e.g., 100°C, have smaller Gibbs free energy. These limitations may be the reason for the relatively small change in the reduction of TOCs of underlaying $TiO_2$ films. However, some specific combinations of $Al_2O_3$ barrier layer films on fixed thickness $TiO_2$ films are needed to evaluate fully the surface porosity model of $TiO_2$ films (Paper **I**).

### 5.1.3 ALD-$Al_2O_3$ thin films

In a third set of experiments, only $Al_2O_3$ barrier layers of different thicknesses ($\sim$ 60 nm, 100–500 nm with 100 nm thickness increment) were coated on Si wafers in order to study their thermo-optical properties. We call this set $S_{C(1-6)}$. We consider here the thinnest $Al_2O_3$ film of thickness $\sim$ 60 nm. A least-square fit of the plotted curve to the data points generates an equation

$$\frac{n^2+2}{n^2-1} = 7.02\times10^{-7}T^2 - 2.28\times10^{-4}T + 3.02, \tag{5.2}$$

where the coefficients of $T^2$ and $T$ have units $^{\circ}C^{-2}$ and $^{\circ}C^{-1}$, respectively. The differentiation of the above equation with respect to $T$ leads to an equation

$$\frac{dn}{dT} = -\frac{(n^2-1)^2}{6n}\left(1.41\times10^{-6}T - 2.28\times10^{-4}\right), \tag{5.3}$$

where the coefficients of $T$ and $T^0$ have units $^{\circ}C^{-2}$ and $^{\circ}C^{-1}$, respectively. The $dn/dT$ values at room temperature ($T$ = 20°C) and at 100°C are $(4.66\pm1.32)\times10^{-5}{}^{\circ}C^{-1}$ and $(2.06\pm1.32)\times10^{-5}{}^{\circ}C^{-1}$, respectively.

Similarly, the fitting of density data points determined for the $Al_2O_3$ film of thickness $\sim$ 60 nm at a wavelength of 640 nm for the temperature range 20–150°C

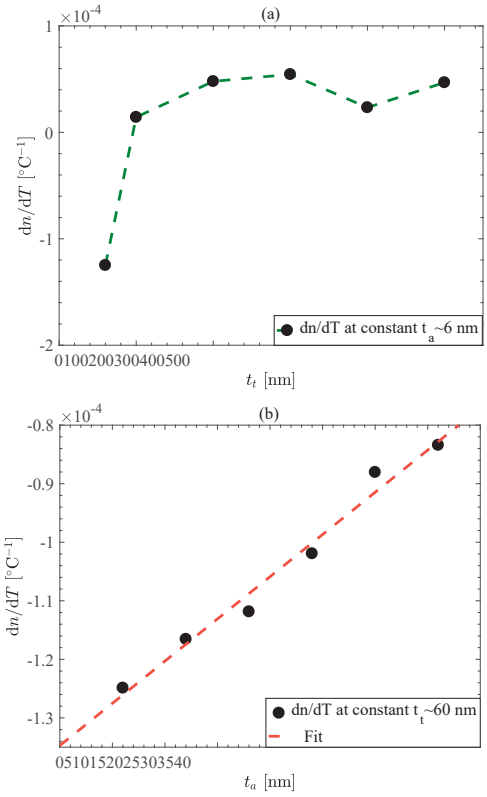


**Figure 5.2:** (a) Thermal dependence of TOCs of various thicknesses of ALD-$TiO_2$ films in the presence of a thin ALD-$Al_2O_3$ barrier layer ($\sim$ 6 nm), (b) Thermal dependence of TOCs of fixed thickness ALD-$TiO_2$ films ($\sim$ 60 nm) in the presence of ALD-$Al_2O_3$ barrier layers of various thicknesses (Paper **I**).

by the Lorentz–Lorenz relation gives an equation

$$\rho(T) = -6.36 \times 10^{-7} T^2 + 2.06 \times 10^{-4} T + 2.72, \tag{5.4}$$

where the units of $\rho(T)$ are $\mathrm{g\,cm^{-3}}$ and the units of the coefficients of $T^2$, $T$, and $T^0$ are $^\circ\mathrm{C}^{-2}\mathrm{g\,cm^{-3}}$, $^\circ\mathrm{C}^{-1}\mathrm{g\,cm^{-3}}$, and $\mathrm{g\,cm^{-3}}$, respectively. The differentiation of Eq. (5.4) with respect to $T$ gives

$$\frac{\mathrm{d}\rho(T)}{\mathrm{d}T} = -1.27 \times 10^{-6} T + 2.06 \times 10^{-4}. \tag{5.5}$$

where the units of $\mathrm{d}\rho(T)/\mathrm{d}T$ are $^\circ\mathrm{C}^{-1}\mathrm{g\,cm^{-3}}$ and the units of the coefficients of $T$ and $T^0$ are $^\circ\mathrm{C}^{-2}\mathrm{g\,cm^{-3}}$ and $^\circ\mathrm{C}^{-1}\mathrm{g\,cm^{-3}}$, respectively. The $\mathrm{d}\rho(T)/\mathrm{d}T$ values at room temperature and at 100°C are $(1.81 \pm 0.51) \times 10^{-4}$ $\mathrm{g\,cm^{-3}}$ $^\circ\mathrm{C}^{-1}$ and $(7.88 \pm 5.12) \times 10^{-5}$ $\mathrm{g\,cm^{-3}}$ $^\circ\mathrm{C}^{-1}$, respectively.

By plotting the variation of $\mathrm{d}n/\mathrm{d}T$ with the thickness of $Al_2O_3$ (Fig. 5.2(b)) leads to a linear fit equation

$$\frac{\mathrm{d}n}{\mathrm{d}T} = 1.44 \times 10^{-6} t_\mathrm{a} - 1.35 \times 10^{-4}. \tag{5.6}$$

Here, $t_a$ is the thickness of $Al_2O_3$ barrier layer and the units of the coefficients $t_a$ and $t_a{}^0$ are $^\circ C^{-1}nm^{-1}$ and $^\circ C^{-1}$, respectively (Paper **I**).

### 5.1.4 ALD-$TiO_2$–$Al_2O_3$ thin bilayer films

In order to further stabilize the thermo-optic coefficients of thin $TiO_2$ films, a set of $Al_2O_3$ diffusion barrier layers of different thicknesses (10–70 nm with 10 nm thickness interval) were deposited on fixed thickness $TiO_2$ ($\sim$ 100 nm) films on Si wafers by ALD. A schematic of $TiO_2$–$Al_2O_3$ bilayer films with ellipsometric illumination geometry is shown in Fig. 5.3.

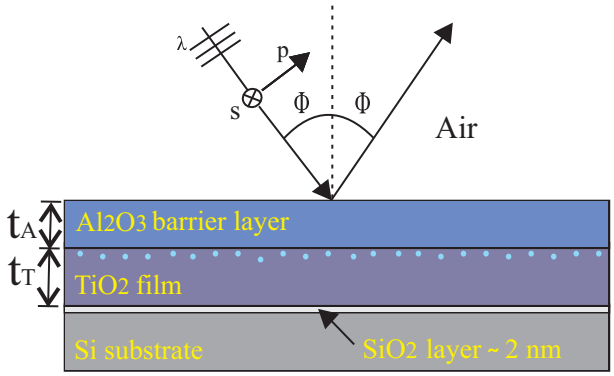


**Figure 5.3:** Schematic of $TiO_2$ and $Al_2O_3$ bilayer films grown by atomic layer deposition (ALD) on a Si substrate. The illumination geometry in ellipsometric measurements is also shown (Paper **II**).

The thickness-, wavelength- and temperature-dependent refractive indices of $TiO_2$–$Al_2O_3$ thin bilayer films were measured by VASE for a wavelength range 380–1800 nm with scan step of 5 nm, temperature range 22–102°C with 10°C temperature interval for three angles of incidence (59°, 67°, and 75°). The thickness and temperature-dependent refractive indices of bilayer films were modeled by the Cauchy model. The optical constants and their corresponding uncertainties of these bilayer films were extracted at a wavelength of 640 nm using the Cauchy dispersion formula (4.10) and the corresponding uncertainty equation

$$\sigma\left[n\left(\lambda\right)\right] = \left[\left(\sigma A\right)^2 + \left(\frac{\sigma B}{\lambda^2}\right)^2 + \left(\frac{\sigma C}{\lambda^4}\right)^2\right]^{\frac{1}{2}}. \tag{5.7}$$

The TOC of each film in the bilayers together with their corresponding uncertainties were obtained by using the refractive index data and corresponding uncertainties determined by Eqs. (4.10) and (5.7) at a wavelength of 640 nm by using a polynomial fitting algorithm [142, 143]. Figure 5.4 shows the TOCs of $TiO_2$ and $Al_2O_3$ films in bilayer films as a function of $Al_2O_3$ film thickness $t_A$. It can be seen that TOCs of $Al_2O_3$ films have positive values when the thickness $t_A$ is 30 nm or more and the TOCs are nearly stable at higher $t_A$ thickness values. On the other hand, the underlying $TiO_2$ films in turn attain positive TOCs values when the $t_A$ is 30 nm or more. This shows that $Al_2O_3$ films at 30 nm thickness and above are nearly pin-hole free, which not only helps attaining the positive TOCs values for $TiO_2$ films

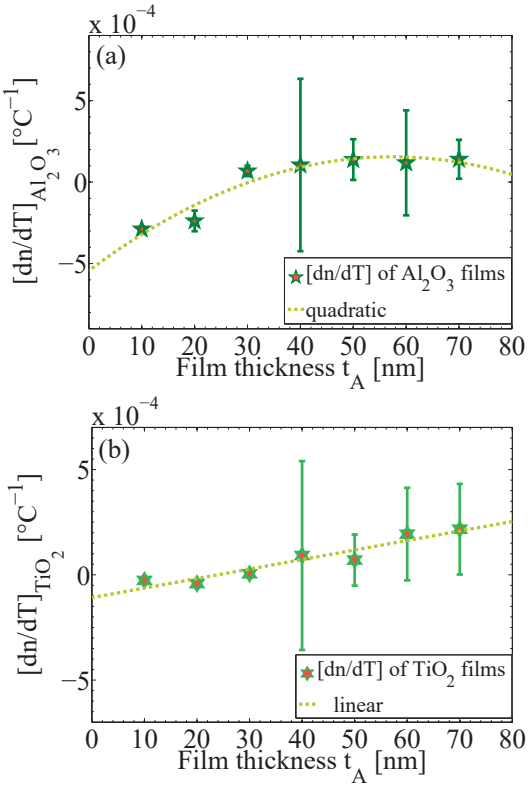


**Figure 5.4:** Thermo-optic coefficients of (a) $Al_2O_3$ films of different thicknesses and (b) $TiO_2$ films of fixed thickness in the presence of $Al_2O_3$ films of different-thickness in bilayer combinations (Paper **II**).

but also help to preserve their inherent optical properties. A linear fit of the $TiO_2$ TOCs as a function of $Al_2O_3$ thickness $t_A$ leads to an equation

$$\left[\frac{dn}{dT}\right]_{TiO_2} = 6.7 \times 10^{-6} t_A - 2.2 \times 10^{-4}. \quad (5.8)$$

Here, the slope $6.7 \times 10^{-6}$ has dimensions $^\circ C^{-1}$ $nm^{-1}$, and $^\circ C^{-1}$ for $-2.2 \times 10^{-4}$. TOCs of a 100 nm $TiO_2$ and a 30 nm $Al_2O_3$ thin films in a bilayer calculated at $T = 62^\circ C$ and wavelength 640 nm are $(0.048 \pm 0.134) \times 10^{-4}$ $^\circ C^{-1}$ and $(0.680 \pm 0.313) \times 10^{-4}$ $^\circ C^{-1}$, respectively (Paper **II**). The modeling of the thermal properties of thin films and bilayers by WVASE32 software is further discussed in more detail in Papers **I** and **II**.

## 5.2 BURIED NANOSTRUCTURES

In this section, we present a method for the fabrication of corrugated surface profile nano-structures that are buried by growing a $TiO_2$ cover layer by atomic layer deposition. In particular, here we present and discuss briefly the theoretical and experimental results related to the buried GMRFs, which have been discussed in

more detail in Paper **III**. It is, however, worth stressing that the same ideas and techniques are far more widely applicable. For the idea to work, the surface profile to be buried needs to be at least quasi-periodic, with a local period of the order of the visible wavelength or less (meaning local periodicity in sub-micrometer scale). This condition is satisfied in, e.g., resonance-domain diffractive optics, photonic-crystal structures, and multilayered quasi-planar chiral metamaterials.

Selection of appropriate process parameters and the conformal nature of $TiO_2$ growth by ALD results in a smooth and nearly flat-top surface profile. The resulting profile of the buried nano-structure is hard in nature, so that it can be easily cleaned without damage, which makes the nano-structure reusable. We discuss a strategy of how to design buried nanostructures starting from corrugated surface profiles and transforming them into volume structures. We then proceed to experimental verification of these structures by describing the fabrication method, and to test the results of GMRF structures that behave as narrow-band spectral filters based on the guided-mode resonance effect even after being buried completely by dielectric cover layers.

### 5.2.1 Design of buried GMRFs

The general design principle of grating structures to be realized by the proposed fabrication technique is illustrated in Fig. 5.5(a). Here a periodic initial surface profile $h(x)$ of period $d$ and refractive index $n_r$ on a flat substrate of refractive index $n_s$ is shown. The surface profile $h(x)$ is coated conformally by ALD with a material of refractive index $n_c$. The ALD process starts by depositing monolayers, and it continues with multilayers until the grooves in the original nano-structure $h(x)$ are eventually filled and the modulation of the top surface becomes smoother and weakly modulated with almost flat-top surface profile, which is illustrated by simulating conformal growth of, e.g., ALD-$TiO_2$ in Fig. 5.5(b).

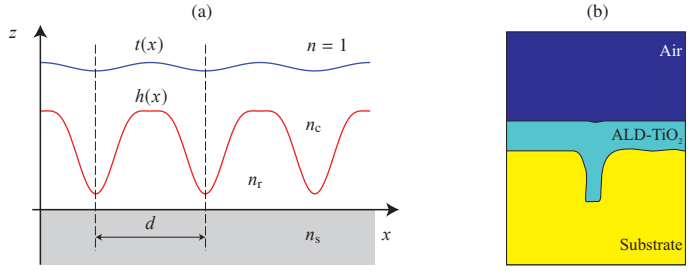


**Figure 5.5:** (a) The concept of simulated ALD conformal growth of a material on a nano-structured surface profile (red line) until a desired slightly modulated top profile (blue line) is obtained. (b) Simulation of a 50-nm-thick $TiO_2$ layer grown by ALD on a real fabricated grating, extracted from an SEM picture (Paper **III**).

Sometimes, owing to the high aspect ratio of the structures, where the structure height is equal to or greater than the period, are desired. Such high aspect ratio structures are fragile in nature: they can easily break if not handled carefully and are also prone to cleaning difficulties after contamination. This can make the element

non-usable after, e.g., a sensing process. This situation is tackled by burying the high-aspect-ratio structures with a solid material. Basically, it is the internal structure that defines the primary optical function, whereas the high index and solid filling material contributes partially to the diffraction characteristics. Sometimes, due to high refractive index of the filling material, high reflection losses are observed although the top layer has an essentially flat surface profile and its thickness can be adjusted to minimize such losses. This situation can be tackled by deposition of dielectric layers with suitable refractive indices on top of the cover layer material by ALD. The whole process of transforming a basic surface relief element into a volume-type is depicted in Figs. 5.6(a–c).

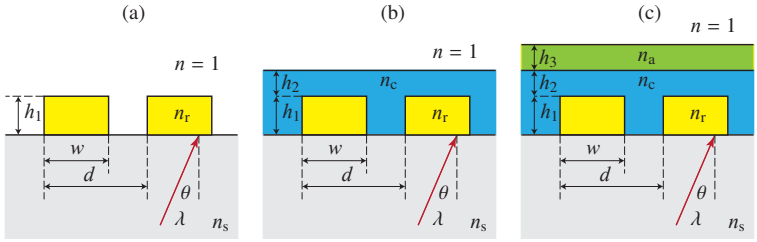


**Figure 5.6:** (a) A bare binary grating illuminated by a plane wave from substrate side. (b) A binary grating buried completely by ALD conformal growth of a material with refractive index $n_c$. (c) A buried grating coated with an additional ALD-grown layer of material with refractive index $n_a$. We consider $n_s \approx n_r$ and $n_c > n_a > n_s > n$ (Paper **III**).

### 5.2.2 Main design results of ALD-$TiO_2$ buried GMRFs

We used FMM to find optimal structural parameters for inorganic GMRFs buried with $TiO_2$ cover layers. The two designs that are realized are named GMRF-I and GMRF-II. The structural parameters of GMRF-I are $d = 310$ nm, $w = 250$ nm (fill factor $f = 0.81$), $h_1 = 85$ nm, and $h_2 = 120$ nm. The parameters of GMRF-II are $d = 310$ nm, $w = 225$ nm ($f = 0.73$), $h_1 = 75$ nm, and $h_2 = 95$ nm. The incidence angle $\theta = 18^\circ$ is the same for both grating types. The simulated TE and TM spectral variations as a result of increasing $TiO_2$ thickness for both types of GMRFs till these are buried completely are shown in Fig. 5.7.

### 5.2.3 Main experimental results

SEM images of the fabricated and buried GMRF-I and II after all polymer testings are shown in Fig. 5.8. The images demonstrate that a nearly flat top surface is indeed achieved by the ALD burying process.

The spectral measurements were performed with a variable angle spectroscopic ellipsometer (VASE) at 18° incident angle for both TE- and TM-polarizations for reflection spectra in the wavelength range 550 nm $\leqslant \lambda \leqslant$ 700 nm. The simulated and measured TE- and TM-reflectance spectra are in close agreement and the results are shown and discussed in detail in Paper **III**. In order to test the fabricated and

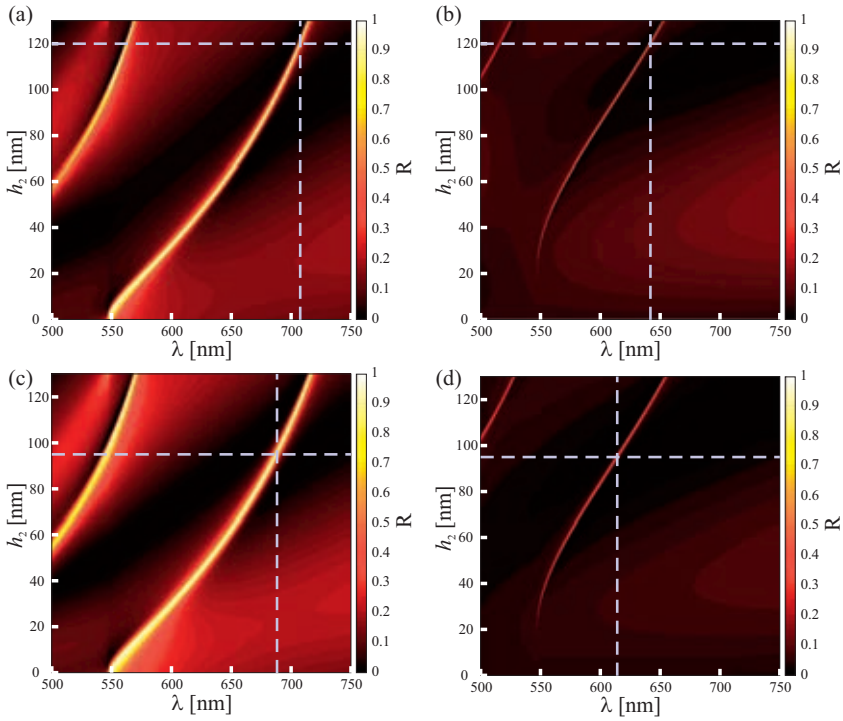


**Figure 5.7:** Simulated spectral variations as a function of increasing $TiO_2$ thickness for GMRF-I for (a) TE-polarization and (b) TM-polarization. Similarly, for GMRF-II, in (c) TE-polarization and in (d) TM-polarization (Paper **III**).

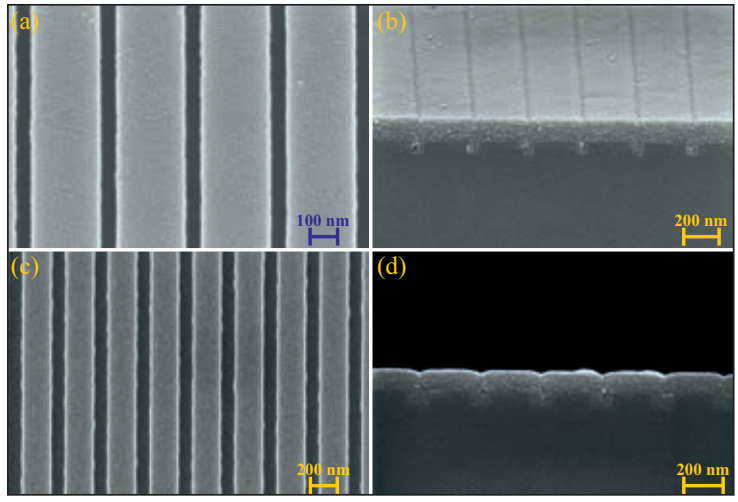


**Figure 5.8:** SEM images of the top surfaces of (a) GMRF-I and (c) GMRF-II before ALD-$TiO_2$ deposition, respectively. (b) and (d) are the cross-sectional images after GMRF-I and II are buried completely by ALD-$TiO_2$ (Paper **III**).

buried GMRFs in sensing applications, we assume that an additional thin layer of the material to be sensed is located on top of the buried grating, mimicking a structure in Fig. 5.6(c). Both GMRF-I and GMRF-II produce sharp TE- and TM-resonances theoretically, the positions of which depend on the thickness $h_3$ and refractive index $n_a$ of an additional layer.

A total of three polymeric materials, Polymethyl Methacrylate (PMMA, $n_a \simeq 1.47$), Polyvinyl Alcohol (PVA, $n_a \simeq 1.53$), and AZ nLOF 2070 (nLOF, $n_a \simeq 1.63$) with approximate thickness of $h_3 \simeq 65$ nm that act as cladding media were tested separately on GMRF-I and II for both TE- and TM-polarizations. The TE- and TM-reflectance spectra of bare buried GMRF-I and II were measured each time (after polymer cleaning in harsh environments) and both spectra corresponded well with the simulations after every cleaning step. This demonstrates the strength and re-usability of the fabricated buried structures and opens remarkable possibilities in the sensing domain and many other areas of diffractive optics. Simulations and experimental sensing results for GMRF-I and II for both TE- and TM-polarizations are presented in Fig. 5.9.

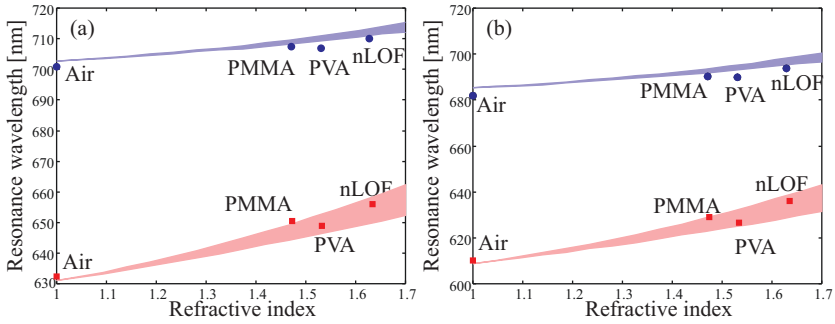


**Figure 5.9:** Experimental sensing results of three different polymers tested separately on the same GRMF for both TE-polarizations (blue-colored strip) and TM-polarizations (red-colored strip). (a) GMRF-I. (b) GMRF-II (Paper **III**).

The measured sensitivities (the resonant wavelength shift as a function of refractive index variation of cladding medium) for TE- and TM-polarizations are 14 nm/RIU and 35 nm/RIU, respectively for GMRF-I. Whereas, for GMRF-II, the sensitivities for TE- and TM-polarizations are 17 nm/RIU and 38 nm/RIU, respectively. It is obvious from the measured sensitivity results that the fabricated and tested buried GMRF devices are twice more sensitive when illuminated under TM-polarization than under TE-polarization.

# 6 Conclusions and outlook

In this chapter, we provide conclusions of the work reported above and discuss ideas that can be realized in the future on the basis of the results that have been achieved.

## 6.1 CONCLUSIONS

The first part of the work demonstrated in this thesis (based on Papers **I** and **II**) deals substantially with the investigation of the changes induced in the optical properties of high index optical grade thin amorphous $TiO_2$ and $Al_2O_3$ films (single as well as bilayers) fabricated by atomic layer deposition (ALD) technique and characterized in thermal environment. Thermo-optical properties of high index optical grade ALD-$TiO_2$, ALD-$Al_2O_3$ thin films, and their bilayer combinations were characterized by variable angle spectroscopic ellipsometry. The second part of the thesis work (Paper **III**) deals with the use of ALD-$TiO_2$ films to make robust, nearly flat-top, and buried guided mode resonance filters for sensing applications. A short summary of the main outcomes of the thesis work and Papers **I–III**, appended in this thesis, is given below.

### 6.1.1 Thin films

Paper **I** involves a broad investigation of the determination of thermo-optical properties of different thicknesses of ALD-$TiO_2$ films in the presence of very thin ALD-$Al_2O_3$ films, thin ALD-$TiO_2$ films of fixed thickness with gradual increase of thin ALD-$Al_2O_3$ over-layer films, and single layers of ALD-$Al_2O_3$ of different thicknesses. It is found that the first bilayer set of different thickness ALD-$TiO_2$ films ($\sim$ 60–500 nm) in the presence of fixed thickness thin ALD-$Al_2O_3$ films ($\sim$ 6 nm) does not make a considerable difference in stabilizing TOCs due to a wide-spread depletion region (porosity region) underneath the barrier films or the existence of tiny pinholes on ALD-$Al_2O_3$ films. In the second bilayer set, ALD-$Al_2O_3$ barrier films of regular thickness ($\sim$ 6–36 nm) are deposited on fixed thickness ALD-$TiO_2$ films ($\sim$ 60 nm), an overall 33% reduction in the TOCs of ALD-$TiO_2$ films at $\sim$ 36 nm ALD-$Al_2O_3$ film thickness has been achieved, which still depicts the strong dominance of widespread depletion region under the barrier films, the existence of pinhole or surface defects owing to very thin nature of ALD-$Al_2O_3$ barrier films. In the third set, ALD-$Al_2O_3$ barrier films of different thicknesses ($\sim$ 60–500 nm) are exploited that exhibit positive TOCs due to slow decrease in their densities with almost no surface defects. The opposite nature of TOCs of both thin ALD-$TiO_2$ and $Al_2O_3$ films makes them suitable to be exploited in athermal device applications.

The investigation of thermo-optical properties of fixed thickness ALD-$TiO_2$ films (thickness $\sim$ 100 nm) in the presence of gradual increment of thin ALD-$Al_2O_3$ films (10–70 nm with 10 nm thickness interval) is continued in Paper **II** in order to make the TOCs of under-layered $TiO_2$ films positive in ALD-$TiO_2$–$Al_2O_3$ bilayer structures. The most effective response in terms of stabilizing the refractive indices of $TiO_2$ films over varying temperatures and consequently the positive TOC value is

obtained when the thickness of ALD-$Al_2O_3$ barrier film is changed from 20 nm to 30 nm. The successful demonstration by the selection of thickness specific combinations of ALD-$TiO_2$–$Al_2O_3$ bilayer films not only show improvement in optical and thermo-optical ($dn/dT$) properties of ALD-$TiO_2$ films but also exhibits an increase in its TOC value when the thickness of ALD-$Al_2O_3$ barrier film is increased linearly. This real breakthrough in thin barrier layers may have plenty of applications in nanophotonics devices where temperature-dependent operation is a nuisance.

### 6.1.2 GMRFs

Paper **III** deals with the theoretical and experimental investigations of ALD-$TiO_2$ buried flat-top guided mode resonance filters (GMRF-I and II) for sensing applications. In this work, an ALD fabrication technique to bury a nano-structured surface-corrugated resonance-domain diffractive element into a solid high-index material (a volume-type-element) is proposed. It offers a way to overcome problems with fragileness and environmental sensitivity of high-aspect-ratio surface-corrugated diffractive nano-structures. The proposed technique is used to design, fabricate, and characterize ALD-$TiO_2$ buried and nearly flat-top GMRFs, to be used in sensing applications. The resulting buried and nearly flat-top surface profiles of GMRFs can be easily cleaned before their re-use with an another sensing material, without any noticeable damage to the structures or deterioration in the optical responses. The proposed method is expected to find widespread use in nanophotonics.

## 6.2 DIRECTIONS FOR FUTURE WORK

Good stability of optical properties of thinner ALD-$TiO_2$ films over varying temperatures has been achieved by the use of ALD-$Al_2O_3$ over-layer films. The thermo-optical properties of ALD-$Al_2O_3$ films of different thicknesses have also been investigated, which possess positive TOCs but also help to stabilize, protect, and preserve the inherent optical properties of underlaying ALD-$TiO_2$ films over varying temperatures, apparent damages, and various other environmental changes. Such ALD-grown bilayers and nanostacks find use in multilayer stacked inorganic or hybrid organic-inorganic athermal waveguides, narrowband filtering, and various other optics and photonics device applications where the environmental changes have significant effects on the device operation.

GMRFs buried by ALD-$TiO_2$ films, which result in nearly flat-top surface profiles are ideal for sensing applications. Such buried and nearly flat-top structures offer easy cleaning and can be used a number of times without any significant alteration in their designed optical properties. Apart from sensing applications, such robust structures can find applications in, e.g., photonic-crystal structures and multilayered quasi-planar chiral metamaterials. In particular, the ALD-based burial technique appears useful in the infrared optical region, where diffractive elements made of semiconductor materials are a natural choice. However, such elements have high reflection losses due to the large refractive-index contrast between semiconductors and air. ALD-coating or burying of these elements with single or multiple layers of materials such as $TiO_2$, $Al_2O_3$, or $SiO_2$ could significantly reduce these losses and also provide additional degrees of freedom for element design.

In addition to the work presented in this thesis, the preliminary studies of the optical properties of different phases of $TiO_2$ thin films (amorphous as well as crystalline) fabricated by ALD on silica substrates, measured by prism coupler as a

function of temperature, and characterized by XRD, have also been done. This work could open up new possibilities in the realm of crystal and optical sciences.

# BIBLIOGRAPHY


[1] J. T. Andrews, E. A. Vangieson, R. E. Enstrom, J. R. Appert, J. B. Kirk, and N. W. Carlson, "Buried Grating Distributed Feedback Laser at $\lambda$=1.51 $\mu$m," *IEEE Proceedings of Third International Conference Indium Phosphide and Related Materials, Cardiff, UK* 106–109 (1991).

[2] S. M. George, "Atomic Layer Deposition: An Overview," *Chem. Rev.* **110**, 111–131 (2010).

[3] M. R. Saleem, R. Ali, M. B. Khan, S. Honkanen, and J. Turunen, "Impact of atomic layer deposition to nanophotonic structures and devices," *Front. Mater.* **1**, 1–15 (2014).

[4] M. R. Saleem, P. Silfsten, S. Honkanen, and J. Turunen, "Thermal properties of $TiO_2$ films grown by atomic layer deposition," *Thin Solid Films* **520**, 5442–5446 (2012).

[5] M. D. Groner, S. M. George, R. S. McLean, and P. F. Carcia, "Gas diffusion barriers on polymers using $Al_2O_3$ atomic layer deposition," *Appl. Phys. Lett.* **88**, 051907 (2006).

[6] P. F. Carcia, R. S. McLean, M. H. Reilly, M. D. Groner, and S. M. George, "Ca test of $Al_2O_3$ gas diffusion barrier layerss grown by atomic layer deposition on polymers," *Appl. Phys. Lett.* **89**, 031915 (2006).

[7] L. Miotti, R. P. Pezzi, M. Copel, C. Krug, and I. J. R. Baumvol, "Atomic transport and integrity of $Al_2O_3$(2.0 nm)/$HfO_2$(2.5 nm) gate stacks on Si," *Appl. Phys. Lett.* **90**, 052913 (2007).

[8] A. A. Dameron, S. D. Davidson, B. B. Burton, P. F. Carcia, R. S. McLean, and S. M. Geroge, "Gas Diffusion Barriers on Polymers Using Multilayers Fabricated by $Al_2O_3$ and Rapid $SiO_2$ Atomic Layer Deposition," *J. Phys. Chem. C* **112**, 4573–4580 (2008).

[9] P. F. Carcia, R. S. McLean, M. D. Groner, A. A. Dameron, and S. M. George, "Gas diffusion ultrabarriers on polymer substrates using $Al_2O_3$ atomic layer deposition and SiN plasma-enhanced chemical vapor deposition," *J. Appl. Phys.* **106**, 023533 (2009).

[10] T. Hirvikorpi, M. Vähä-Nissi, T. Mustonen, E. Iiskola, and M. Karppinen, "Atomic layer deposited aluminum oxide barrier coatings for packaging materials," *Thin Solid Films* **518**, 2654–2658 (2010).

[11] G. Gülşen and M. N. Inci, "Thermal optical properties of $TiO_2$ films," *Opt. Mater.* **18**, 373–381 (2002).

[12] S. Wiechmann and J. Müller, "Thermo–optic properties of $TiO_2$, $Ta_2O_5$ and $Al_2O_3$ films for integrated optics on silicon," *Thin Solid Films* **517**, 6847–6849 (2009).

[13] J. Saarinen, E. Noponen, and J. Turunen, "Guided-mode resonance filters of finite aperture," *Opt. Eng.* **34**, 2560–2566 (1995).

[14] T. Vallius, P. Vahimaa, and J. Turunen, "Pulse deformations at guided-mode resonance filters," *Opt. Express* **10**, 840–843 (2002).

[15] E. Noponen, A. Vasara, J. Turunen, J. M. Miller, and M. R. Taghizadeh, "Synthetic diffractive optics in the resonance domain," *J. Opt. Soc. Am. A* **9**, 1206–1213 (1992).

[16] J. Turunen, E. Noponen, and E. Tervonen, "Resonance-domain diffractive optics," *Optics & Photonics News* **4**, 29–30 (1993).

[17] J. Turunen, M. Kuittinen, and F. Wyrowski, *Diffractive optics: electromagnetic approach* (Elsevier, Amsterdam, 2009), in Progress in Optics, Vol. 40, E. Wolf, ed.

[18] M. R. Taghizadeh, P. Blair, B. Layet, I. M. Barton, A. J. Waddie, and N. Ross, "Design and fabrication of diffractive optical elements," *Microelectron. Eng.* **34**, 219–242 (1997).

[19] H. Li, Z. Hang, Y. Qin, Z. Wei, L. Zhou, Y. Zhang, H. Chen, and C. T. Chan, "Quasi-periodic planar metamaterial substrates," *Appl. Phys. Lett.* **86**, 121108 (2005).

[20] F. Capolino, *Theory and Phenomena of Metamaterials* (CRC Press, Boca Raton, FL, USA, 2009).

[21] W. Cai and V. Shalaev, *Optical Metamaterials: Fundamentals and Applications* (Springer-Verlag, New York, USA, 2010).

[22] M. Ohring, *The Materials Science of Thin Films* (Acadmeic Press, San Diego, California, USA, 1992).

[23] A. Piegari and F. Flory, *Optical thin films and coatings* (Woodhead Publishing Limited, Cambridge, UK, 2013).

[24] P. K. Tien, "Light Waves in Thin Films and Integrated Optics," *Appl. Opt.* **10**, 2395–2413 (1971).

[25] K. L. Choy, "Chemical vapour deposition of coatings," *Prog. Mater. Sci.* **48**, 57–170 (2003).

[26] J.-O. Carlsson and P. M. Martin, *Chemical Vapor Deposition* (William Andrew Publishing, Boston, USA, 2010), Chapter 7 in Handbook of Deposition Technologies for Films and Coatings.

[27] K. Seshan, *Handbook of Thin-Film Deposition Processes and Techniques* (William Andrew Publishing, Norwich, New York, U.S.A, 2002).

[28] P. M. Martin, *Deposition Technologies: An Overview* (William Andrew Publishing, Boston, USA, 2010), Chapter 1 in Handbook of Deposition Technologies for Films and Coatings.

[29] G. N. Parsons, J. W. Elam, S. M. George, S. Haukka, H. Jeon, W. M. M. E. Kessels, M. Leskelä, P. Poodt, M. Ritala, and S. M. Rossnagel, "History of atomic layer deposition and its relationship with the American Vacuum Society," *J. Vac. Sci. Technol. A* **31**, 050818 (2013).

[30] R. W. Johnson, A. Hultqvist, and S. F. Bent, "A brief review of atomic layer deposition: from fundamentals to applications," *Mater. Today* **17**, 237–246 (2014).

[31] Atomic Layer Deposition, `https://beneq.com/en/thin-films/technology/atomic-layer-deposition` (visited on 2018-09-19).

[32] A. Pakkala and M. Putonen, *Atomic Layer Deposition* (William Andrew Publishing, Boston, USA, 2010), Chapter 8 in Handbook of Deposition Technologies for Films and Coatings.

[33] A. Szeghalmi, M. Helgert, R. Brunner, F. Heyroth, U. Gösele, and M. Knez, "Atomic layer deposition of $Al_2O_3$ and $TiO_2$ multilayers for applications as bandpass filters and antireflection coatings," *Appl. Opt.* **48**, 1727–1732 (2009).

[34] R. Ali, *Thermo-Optical Properties of* $TiO_2$ *and* $Al_2O_3$ *Thin Films* (University of Eastern Finland, 2013), Master thesis.

[35] K. Davis, "Material Review: Alumina ($Al_2O_3$)," *School of Doctoral Studies (European Union) Journal* 109–114 (2010).

[36] E. Marin, L. Guzman, A. Lanzutti, W. Ensinger, and L. Fedrizzi, "Multilayer $Al_2O_3/TiO_2$ Atomic Layer Deposition coatings for corrosion protection of stainless steel," *Thin Solid Films* **522**, 283–288 (2012).

[37] D. R. Baer and S. Thevuthasan, *Characterization of Thin Films and Coatings* (William Andrew Publishing, Boston, USA, 2010), Chapter 16 in Handbook of Deposition Technologies for Films and Coatings.

[38] H. Xie, F. L. Ng, and X. T. Zeng, "Spectroscopic ellipsometry study of thin film thermo-optical properties," *Thin Solid Films* **517**, 5066–5069 (2009).

[39] D. Halliday, R. Resnick, and J. Walker, *Fundamentals of Physics* (Wiley, New Jersey, 2011).

[40] M. Born and E. Wolf, *Principles of Optics* (Cambridge University Press, Cambridge, United Kingdom, 1999).

[41] J. Turunen, *Diffraction Theory of Microrelief Gratings* (Taylor & Francis, London, 1997), Chapter 2 in Micro-Optics: Elements, Systems and Applications, H. P. Herzig, ed.

[42] A. Vijayakumar and S. Bhattacharya, *Design and Fabrication of Diffractive Optical Elements with MATLAB* (SPIE Press, 2017).

[43] I. Minin and O. Minin, *Diffractive Optics and Nanophotonics: Resolution Below the Diffraction Limit* (Springer International Publishing AG, Switzerland, 2016).

[44] S. Martellucci and A. N. Chester, *Diffractive Optics and Optical Microsystems* (Springer US, 1997).

[45] M. R. Saleem, *Resonant waveguide gratings by replication and atomic layer deposition*, PhD thesis (University of Eastern Finland, 2012).

[46] C.-L. Chen, *FOUNDATIONS FOR GUIDED-WAVE OPTICS* (John Wiley & Sons, Inc., Hoboken, New Jersey, USA, 1997).

[47] A. R. Mickelson, *Guided Wave Optics* (Springer, US, 1993).

[48] R. Halir, P. J. Bock, P. Cheben, A. Ortega-Moñux, C. Alonso-Ramos, J. H. Schmid, J. Lapointe, D.-X. Xu, J. G. Wangüemert-Pérez, Í. Molina-Fernández, and S. Janz, "Waveguide sub-wavelength structures: a review of principles and applications," *Laser Photonics Rev.* **9**, 25–49 (2015).

[49] C. Palmer and E. Loewen, *DIFFRACTION GRATING HANDBOOK* (Newport Corporation, New York, 2005).

[50] M. Nevière and E. Popov, *Light Propagation in Periodic Media: Differential Theory and Design* (Marcel Dekker, Inc., New York, USA, 2003).

[51] R. Petit, *Electromagnetic Theory of Gratings* (Springer-Verlag Berlin Heidelberg, Germany, 1980).

[52] M. A. Golub and A. A. Friesem, "Effective grating theory for resonance domain surface-relief diffraction gratings," *J. Opt. Soc. Am. A* **22**, 1115–1126 (2003).

[53] I. Rashid, H. Butt, A. K. Yetisen, B. Dlubak, J. E. Davies, P. Seneor, A. Vechhiola, F. Bouamrane, and S. Xavier, "Wavelength-Selective Diffraction from Silica Thin-Film Gratings," *ACS Photonics* **4**, 2402–2409 (2017).

[54] H. Kikuta, H. Toyota, and W. Yu, "Optical elements with subwavelength structured surfaces," *Opt. Rev.* **10**, 63–73 (2003).

[55] R. W. Wood, "On a Remarkable Case of Uneven Distribution of Light in a Diffraction Grating Spectrum," *Proc. Phys. Soc. London* **18**, 269–275 (1902).

[56] M. G. Moharam and T. K. Gaylord, "Diffraction analysis of dielectric surface-relief gratings," *J. Opt. Soc. Am.* **72**, 1385–1392 (1982).

[57] T. K. Gaylord and M. G. Moharam, "Planar Dielectric Grating Diffraction Theories," *Appl. Phys. B* **28**, 1–14 (1982).

[58] J. Rahomäki, *Subwavelength photonics for enhanced optical imaging*, PhD thesis (University of Eastern Finland, 2013).

[59] S. T. Chu and S. K. Chaudhuri, "A Finite-Difference Time-Domain Method for the Design and Analysis of Guided-Wave Optical Structures," *J. Lightwave Technol.* **7**, 2033–2038 (1989).

[60] S. Burger, J. Pomplun, and F. Schmidt, *Finite Element Methods for Computational Nano-optics* (Springer, Dordrecht, Netherlands, 2012), In Encyclopedia of Nanotechnology, B. Bhushan, ed.

[61] H. Kim, J. Park, and B. Lee, *Fourier Modal Method and Its Applications in Computational Nanophotonics* (CRC Press, Boca Raton, FL, USA, 2012).

[62] K. Ohira, N. Nunoya, and S. Arai, "Stable Single-Mode Operation of Distributed Feedback Lasers With Wirelike Active Regions," *IEEE J. Sel. Top. Quantum Electron.* **9**, 1166–1171 (2003).

[63] G. A. Evans and J. M. Hammer, *Surface Emitting Semiconductor Lasers and Arrays* (Academic Press, Inc., San Diego, CA, USA, 1993).

[64] P. Modh, J. Backlund, J. Bengtsson, A. Larsson, N. Shimada, and T. Suhara, "Multifunctional gratings for surface-emitting lasers: design and implementation," *Appl. Opt.* **42**, 4847–4854 (2003).

[65] R. Magnusson and S. S. Wang, "New principle for optical filters," *Appl. Phys. Lett.* **61**, 1022–1024 (1992).

[66] S. S. Wang and R. Magnusson, "Theory and applications of guided-mode resonance filters," *Appl. Opt.* **32**, 2606–2613 (1993).

[67] R. Magnusson and S. S. Wang, *Optical guided-mode resonance filter* (US Patent 5,216,680, 1993).

[68] S. Glasberg, A. Sharon, D. Rosenblatt, and A. A. Friesem, "Spectral shifts and line-shapes asymmetries in the resonant response of grating waveguide structures," *Opt. Comm.* **145**, 291–299 (1998).

[69] H. N. Daghestani and B. W. Day, "Theory and Applications of Surface Plasmon Resonance, Resonant Mirror, Resonant Waveguide Grating, and Dual Polarization Interferometry Biosensors," *Sensors* **10**, 9630–9646 (2010).

[70] D. Rosenblatt, A. Sharon, and A. A. Friesem, "Resonant Grating Waveguide Structures," *IEEE J. Quantum. Electron.* **33**, 2038–2059 (1997).

[71] M. R. Saleem, S. Honkanen, and J. Turunen, "Non-polarizing single layer inorganic and double layer organic-inorganic one-dimensional guided mode resonance filters," *Proc. SPIE* **8613**, 86130C (2013).

[72] M. R. Saleem, P. Stenberg, T. Alasaarela, P. Silfsten, M. B. Khan, S. Honkanen, and J. Turunen, "Towards athermal organic-inorganic guided mode resonance filters," *Opt. Express* **19**, 24241–24251 (2011).

[73] E. Wijaya, C. Lenaerts, S. Maricot, J. Hastanin, S. Habraken, J.-P. Vilcot, R. Boukherroub, and S. Szunerits, "Surface plasmon resonance-based biosensors: From the development of different SPR structures to novel surface functionalization strategies," *Curr. Opin. Solid State Mater. Sci.* **15**, 208–224 (2011).

[74] S. McNamara and Y. B. Gianchandani, *MEMS-Based Sensors* (Elsevier Science, 2011), In Comprehensive Semiconductor Science and Technology, R. Fornari, ed.

[75] NANOSENSORS BASED ON METAL AND COMPOSITE NANOPARTICLES AND NANOMATERIALS, `https://www.eolss.net/Sample-Chapters/C05/E6-152-25-00.pdf` (visited on 2018-10-22).

[76] R. Cush, J. M. Cronin, W. J. Stewart, C. H. Maule, J. Molloy, and N. J. Goddard, "The resonant mirror: a novel optical biosensor for direct sensing of biomolecular interactions Part I: Principle of operation and associated instrumentaton," *Biosens. Bioelectron.* **8**, 347–353 (1993).

[77] P. Moyo, J. M. W. Brownjohn, R. Suresh, and S. C. Tjin, "Development of fiber Bragg grating sensors for monitoring civil infrastructure," *Eng. Struct.* **27**, 1828–1834 (2005).

[78] J. Fluitman and T. Pompa, "OPTICAL WAVEGUIDE SENSORS," *Sens. Actuators* **10**, 25–46 (1986).

[79] R. Horváth, H. C. Pedersen, N. Skivesen, D. Selmeczi, and N. B. Larsen, "Optical waveguide sensor for on-line monitoring of bacteria," *Opt. Lett.* **28**, 1233–1235 (2003).

[80] D. D. Nolte, *Optical Interferometry for Biology and Medicine* (Springer-Verlag, New York, USA, 2012).

[81] P. Dasmborský, J. Švitel, and J. Katrlík, "Optical biosensors," *Essays Biochem.* **60**, 91–100 (2016).

[82] J. Vörös, J. J. Ramsden, G. Csúcs, I. Szendrő, S. M. D. Paul, M. Textor, and N. D. Spencer, "Optical grating coupler biosensors," *Biomaterials* **23**, 3699–3710 (2002).

[83] A. J. Cunningham, *Introduction to bioanalytical sensors* (Wiley-Interscience, New York, NY, USA, 1998).

[84] J. Homola, "Present and future of surface Plasmon resonance biosensors," *Anal. Bioanal. Chem.* **377**, 528–539 (2003).

[85] B. Cunningham, B. Lin, J. Qiu, P. Li, J. Pepper, and B. Hugh, "A plastic colorimetric resonant optical biosensor for multiparallel detection of label-free biochemical interactions," *Sens. Actuators B* **85**, 219–226 (2002).

[86] M. R. Saleem, D. Zheng, B. Bai, P. Stenberg, M. Kuittinen, S. Honkanen, and J. Turunen, "Replicable one-dimensional non-polarizing guided mode resonance gratings under normal incidence," *Opt. Express* **20**, 16974–16980 (2012).

[87] M. R. Saleem and R. Ali, *Polymer Resonant Waveguide Gratings* (IntechOpen Limited, London, United Kingdom, 2018), Chapter 15 in Emerging Waveguide Technology.

[88] R. Magnusson, D. Wawro, S. Zimmerman, and Y. Ding, "Resonant photonic biosensors with polarization-based multiparametric discrimination in each channel," *Sensors* **11**, 1476–1488 (2011).

[89] M. J. Madou, *Fundamentals of Microfabrication and nanotechnology–Volume II* (CRC Press, Boca Raton, FL, USA, 2011), 3rd Edition.

[90] S. Landis, *Nano-Lithography* (ISTE Ltd. and John Wiley & Sons, Inc., London, United Kingdom, 2011).

[91] G. R. Suñé, *Electron beam lithography for Nanofabrication*, PhD thesis (Universitat Autònoma de Barcelona, 2008).

[92] T. R. Groves, *Electron beam lithography* (Woodhead Publishing Limited, Cambridge, United Kingdom, 2014), Chapter 3 in Nanolithography The Art of Fabricating Nanoelectronic and Nanophotonic Devices and Systems.

[93] E.-B. Kley, "Continuous profile writing by electron and optical lithography," *Microelectron. Eng.* **34**, 261–298 (1997).

[94] P. Hahmann and O. Fortagne, "50 years of electron beam lithography: Contributions from Jena (Germany)," *Microelectron. Eng.* **86**, 438–441 (2009).

[95] H. Ahmed, "Electron beam lithography for integrated circuit fabrication," *Phys. Technol.* **11**, 169–174 (1980).

[96] A. N. Broers, A. C. F. Hoole, and J. M. Ryan, "Electron beam lithography – Resolution limits," *Microelectron. Eng.* **32**, 131–142 (1996).

[97] C. S. Wu, Y. Makiuchi, and C. Chen, *High-energy Electron Beam Lithography for Nanoscale Fabrication* (IntechOpen Limited, London, United Kingdom, 2010), Chapter 13 in Lithography.

[98] Institute of Photonics: Fabrication of Micro- and Nanostructures for Photonics, `https://www.uef.fi/en/web/photonics/fabrication-of-micro-and-nanostructures-for-photonics` (visited on 2018-10-23).

[99] T. Suntola, "Atomic Layer Epitaxy," *Mater. Sci. Rep.* **4**, 261–312 (1989).

[100] M. Ritala and M. Leskelä, *ATOMIC LAYER DEPOSITION* (Academic Press, San Diego, CA, USA, 2002), Chapter 2 in Handbook of Thin Film Materials: Deposition and Processing of Thin Films.

[101] M. Leskelä and M. Ritala, "Atomic layer deposition (ALD): from precursors to thin film structures," *Thin Solid Films* **409**, 138–146 (2002).

[102] R. Matero, A. Rahtu, M. Ritala, M. Leskelä, and T. Sajavaara, "Effect of water dose on atomic layer deposition rate of oxide thin films," *Thin Solid Films* **368**, 1–7 (2000).

[103] R. L. Puurunen, "A Short History of Atomic Layer Deposition: Tuomo Suntola's Atomic Layer Epitaxy," *Chem. Vap. Deposition* **20**, 1–13 (2014).

[104] FINNISH CENTRE OF EXCELLENCE IN ATOMIC LAYER DEPOSITION, `http://www.aldcoe.fi/events/finald40.html` (visited on 2018-09-17).

[105] H. Kim, H.-B.-R. Lee, and W.-J. Maeng, "Applications of atomic layer deposition to nanofabrication and emerging nanodevices," *Thin Soild Films* **517**, 2563–2580 (2009).

[106] H. Kim, "Atomic layer deposition of metal and nitride thin films: Current research efforts and applications for semiconductor device processing," *J. Vac. Sci. Technol. B.* **21**, 2231–2261 (2003).

[107] H. Kim, "Characteristics and applications of plasma enhanced-atomic layer deposition," *Thin Solid Films* **519**, 6639–6644 (2011).

[108] T. Nam, J.-M. Kim, M.-K. Kim, and H. Kim, "Low-temperature Atomic Layer Deposition of $TiO_2$, $Al_2O_3$, and ZnO Thin Films," *J. Kr. Phys. Soc.* **59**, 452–457 (2011).

[109] R. L. Puurunen, "Surface chemistry of atomic layer deposition: a case study for the trimethylaluminum/water process," *Appl. Phys.* **97**, 121301 (2005).

[110] T. L. Chu, J. R. Szedon, and J. E. Johnson, *Method of depositing titanium dioxide films by chemical vapor deposition* (US patent 3,916,041, 1974).

[111] C. Y. Yuan and D. A. Dornfeld, "Integrated Sustainability Analysis of Atomic Layer Deposition for Microelectronics Manufacturing," *J. Manuf. Sci. Eng.* **132**, 030918 (2010).

[112] J. Leem, I. Park, Y. Li, W. Zhou, Z. Jin, S. Shin, and Y.-S. Min, "Role of HCl in Atomic Layer Deposition of $TiO_2$ Thin Films from Titanium Tetrachloride and Water," *Bull. Korean Chem. Soc.* **35**, 1195–1201 (2014).

[113] A. C. Dillon, A. W. Ott, J. D. Way, and S. M. George, "Surface chemistry of $Al_2O_3$ deposition using $Al(CH_3)_3$ and $H_2O$ in a binary reaction sequence," *Surf. Sci.* **322**, 230–242 (1995).

[114] Beneq TFS 200, `https://beneq.com/en/thin-films/products/ald-research-equipment/beneq-tfs-200` (visited on 2018-10-23).

[115] M. Losurdo, M. Bergmair, G. Bruno, D. Cattelan, C. Cobet, A. de Martino, K. Fleischer, Z. Dohcevic-Mitrovic, N. Esser, M. Galliet, R. Gajic, D. Hemzal, K. Hingerl, J. Humlicek, R. Ossikovski, Z. V. Popovic, and O. Saxl, "Spectroscopic ellipsometry and polarimetry for materials and systems analysis at the nanometer scale: state-of-the-art, potential, and perspectives," *J. Nanopart. Res.* **11**, 1521–1554 (2009).

[116] *A Short Course in Ellipsometry, Guide to Using WVASE32, Software for Spectroscopic Ellipsometry Data Acquisition and Analysis* (J.A. Woollam Co., Inc., Lincoln, NE, USA, 2001).

[117] *VASE Series Ellipsometers, Hardware manual, VASEmanual* (J.A. Woollam Co., Inc., Lincoln, NE, USA, 2003).

[118] R. M. A. Azzam and N. M. Bashara, *Ellipsometry and Polarized Light* (North-Holland Pub. Co., Amsterdam, Nethersland, 1977).

[119] J. A. Woollam, B. Johs, C. M. Herzinger, J. Hilfiker, R. Synowicki, and C. L. Bungay, "Overview of Variable Angle Spectroscopic Ellipsometry (VASE), Part I: Basic Theory and Typical Applications," *Proc. SPIE* **72**, 3–28 (1999).

[120] T. M. El-Agez, A. A. E. Tayyan, and S. A. Taya, "Rotating polarizer-analyzer scanning ellipsometer," *Thin Solid Films* **518**, 5610–5614 (2010).

[121] J. A. Woollam, J. L. Hilfiker, T. E. Tiwald, C. L. Bungay, R. A. Synowicki, D. E. Meyer, C. M. Herzinger, G. L. Pfeiffer, G. T. Cooney, and S. E. Green, "Variable Angle Spectroscopic Ellipsomtery in the Vacuum Ultrviolet," *Proc. SPIE* **4099**, 1–9 (2000).

[122] H. G. Tompkins and W. A. McGahan, *Spectroscopic Ellipsometry and Reflectometry: A User's Guide* (John Wiley & Sons, Inc., New York, USA, 1999).

[123] Optical Constants, `https://www.jawoollam.com/resources/ellipsometry-tutorial/optical-constants` (visited on 2018-10-23).

[124] Optical Characterization By Spectroscopic Ellipsometry, http://grover.mirc.gatech.edu/data/gatech_ellipsometry_seminar-dec_2010.pdf (visited on 2018-10-23).

[125] Y. C. Liu, J. H. Hsieh, and S. K. Tung, "Extraction of optical constants of zinc oxide thin films by ellipsometry with various models," *Thin Solid Films* **510**, 32–38 (2006).

[126] *VASE, Variable Angle Spectroscopic Ellipsometry, Ellipsometry solutions* (J.A. Woollam Co., Inc., Lincoln, NE, USA, 2012).

[127] J. N. Hilfiker, N. Singh, T. Tiwald, D. Convey, S. M. Smith, J. H. Baker, and H. G. Tompkins, "Survey of methods to characterize thin absorbing films with Spectroscopic Ellipsometry," *Thin Solid Films* **516**, 7979–7989 (2008).

[128] VASE Ellipsometer, https://www.jawoollam.com/products/vase-ellipsometer (visited on 2018-10-23).

[129] K. D. Vernon-Parry, "Scanning Electron Microscopy: an introduction," *III-Vs Review* **14**, 40–44 (2000).

[130] D. C. Joy, "Scanning electron microscopy for materials characterization," *Curr. Opin. Solid State Mater. Sci.* **2**, 465–468 (1997).

[131] L. Reimer, *Scanning Electron Microscopy Physics of Image Formation and Microanalysis* (Springer-Verlag Berlin Heidelberg GmbH, Germany, 1998).

[132] R. F. Egerton, *Physical Principles of Electron Microscopy* (Springer International Publishing, Switzerland, 2016).

[133] Experimental Equipment: High-resolution SEM Gemini 1550 (Zeiss AG), https://www.mpikg.mpg.de/152103/3Ausstattung (visited on 2018-10-23).

[134] Metricon Corporation, http://www.metricon.com/ (visited on 2018-07-20).

[135] X-Ray Diffraction Shared Experimental Facility, http://prism.mit.edu/xray/education/reading.html (visited on 2018-07-20).

[136] X-ray Diffraction (XRD) and Scattering, https://www.bruker.com/products/x-ray-diffraction-and-elemental-analysis/x-ray-diffraction.html (visited on 2018-10-23).

[137] F. Moreno-Herrero, J. Colchero, J. Gómez-Herrero, and A. M. Baró, "Atomic force microscopy contact, tapping, and jumping modes for imaging bilogical samples in liquids," *Phys. Rev. E* **69**, 031915 (2004).

[138] F. L. Leite, C. E. Borato, W. T. L. da Silva, P. S. P. Herrmann, O. N. Oliveira, and L. H. C. Mattoso, "Atomic Force Spectroscopy on Poly(o-ethoxyaniline) Nanostructured Films: Sensing Nonspecific Interactions," *Microsc. Microanal.* **13**, 304–312 (2007).

[139] K. B. Crozier, G. G. Yaralioglu, F. L. Degertekin, J. D. Adams, S. C. Minne, and C. F. Quate, "Thin film characterization by atomic force microscopy at ultrasonic frequencies," *Appl. Phys. Lett.* **76**, 1950–1952 (2000).

[140] ScanAsyst: Self-Optimizing AFM for High-Resolution Imaging, https://www.bruker.com/products/surface-and-dimensional-analysis/atomic-force-microscopes/modes/modes/imaging-modes/scanasyst.html (visited on 2018-10-23).

[141] C. Kittel, *Introduction to Solid State Physics* (John Wiley & Sons, Inc., USA, 1996).

[142] MATLAB, (The MathWorks Inc.:, Natick, MA, USA, 2012), version R2012a (7.14.0.739).

[143] W. H. Press, B. P. Flannery, S. A. Teukolsky, and W. T. Vetterling, *Numerical Recipes: The Art of Scientific Computing* (Cambridge University Press, Cambridge, UK, 1986).

# A Appendix

## A.1 LIST OF ADDITIONAL PUBLICATIONS

In addition, the author has authored and co-authored the following peer-reviewed journal articles and international conference papers:

**i** M. R. Saleem, **R. Ali**, M. B. Khan, S. Honkanen and J. Turunen, "Impact of atomic layer deposition to nanophotonic structures and devices," *Front. Mater.* **1**, 1–15 (2014).

**ii** M. R. Saleem, **R. Ali**, S. Honkanen, J. Turunen, "Effect of waveguide thickness layer on spectral resonance of a Guided Mode Resonance Filter," in *IEEE Proceedings of 2014 11th International Bhurban Conference on Applied Sciences & Technology (IBCAST), Islamabad, Pakistan*, 39–43 (2014).

**iii** M. R. Saleem, **R. Ali**, S. Honkanen, and J. Turunen, "Determination of thermo-optic properties of atomic layer deposited thin $TiO_2$ films for athermal resonant waveguide gratings by spectroscopic ellipsometry," *Proc. SPIE* **9130**, 1–8 (2014).

**iv** M. R. Saleem, **R. Ali**, A. Nisar, "Impact of Atomic Layer Deposition to The Fabrication of Athermal Guided Mode Resonance Filters," in *IEEE Proceedings of 2015 12th International Bhurban Conference on Applied Sciences & Technology (IBCAST), Islamabad, Pakistan*, 34–39 (2015).

**v** M. R. Saleem, **R. Ali**, S. Honkanen and J. Turunen, "Design and fabrication of sub-wavelength athermal resonant waveguide replicated gratings on different polymer substrates," *Proc. SPIE* **9374**, 1–7 (2015).

**vi** **R. Ali**, M. R. Saleem, S. Honkanen, "Temperature-induced changes in optical properties of thin film $TiO_2$–$Al_2O_3$ bi-layer structures grown by atomic layer deposition," *Proc. SPIE* **9749**, 1–8 (2016).

**vii** A. Shah, P. Stenberg, L. Karvonen, **R. Ali**, S. Honkanen, H. Lipsanen, N. Peyghambarian, M. Kuittinen, Y. Svirko & T. Kaplas, "Pyrolytic carbon coated black silicon," *Sci. Rep.* **6**, 25922 (2016).

**viii** M. R. Saleem, **R. Ali**, S. Honkanen and J. Turunen, "Bio-molecular sensors based on guided mode resonance filters," *IOP Conf. Ser.: Mater. Sci. Eng.* **146**, 012030 (2016).

**ix** K. J. Brobbey, J. Haapanen, M. Gunell, M. Toivakka, J. M. Mäkelä, E. Eerola, **R. Ali**, M. R. Saleem, S. Honkanen, J. Bobacka, J. J. Saarinen, "Controlled time release and leaching of silver nanoparticles using a thin immobilizing layer of aluminum oxide," *Thin Solid Films* **645**, 166–172 (2018).

**x** A. Raza, S. Clemmen, M. de Goede, **R. Ali**, P. Hua, S. M. Garcia-Blanco, S. Honkanen, J. S. Wilkinson, and R. Baets, "The performance of High-Index-Contrast Photonics Platforms for On-Chip Raman Spectroscopy," *European Conference on Integrated Optics (ECIO'2018)*, 35–37 (2018).

**xi** M. R. Saleem and **R. Ali**, "Polymer Resonant Waveguide Gratings In book: Emerging Waveguide Technology," *IntechOpen Limited, London, UK*, Chapter 15, pp. 277–294 (2018).

**xii** K-E. Peiponen, R. Räty, U. Ishaq, S. Pélisset, **R. Ali**, "Outlook on optical identification of micro- and nanoplastics in aquatic environments," *Chemosphere* **214**, 424–429 (2019).

**xiii** A. S. Saushin, R. G. Zonov, E. V. Aleksandrovich, K. G. Mikheev, **R. Ali**, V. V. Vanyukov and G. M. Mikheev, "Influence of electrochemical hydrogenation on the circular photocurrent in the Ag/Pd nanocomposite," *Phys. Status Solidi B*, 1800671 (2019).

## A.2 CONFERENCE PARTICIPATIONS

Also, the author has participated and presented his research work in the following conferences:

**i** *Optics Days* (Helsinki, Finland, 2013) (**Poster**)

**ii** *SPIE Photonics Europe* (Brussels, Belgium, 2014) (**Talk**)

**ii** *European Optical Society Annual Meeting (EOSAM14)* (Berlin, Germany, 2014) (**Talk**)

**iv** *The Eleventh Japan-Finland Joint Symposium on Optics in Engineering (OIE'15)* (Joensuu, Finland, 2015) (**Poster**)

**v** *SPIE Photonics West* (San Francisco, California, United States, 2016) (**Talk**)

**vi** *European Optical Society Annual Meeting (EOSAM16)* (Berlin, Germany, 2016) (**Poster**)

**vii** *Symposium on Future Prospects for Photonics* (Tampere University of Technology (TUT), Tampere, Finland, 2016) (**Poster**)

**RIZWAN ALI**

*This thesis is focused on exploring the thermally induced changes in the optical properties of $TiO_2$ and $Al_2O_3$ thin films, and their bilayers fabricated by Atomic Layer Deposition (ALD) technique and characterized by a Variable Angle Spectroscopic Ellipsometer (VASE) in terms of, e.g., Thermo-Optic Coefficients (TOCs). The negative thermo-optical behavior of thin ALD-$TiO_2$ films is controlled by the use of thin ALD-$Al_2O_3$ films, which intrinsically carry positive TOCs, as cover-layers. The thin ALD-$Al_2O_3$ films in $TiO_2$–$Al_2O_3$ bilayers act as impermeable barrier layers and help to stabilize the optical characteristics of underlying $TiO_2$ thin films in varying thermal environments. In addition, sub-wavelength Guided Mode Resonance Filters (GMRFs), buried with ALD-$TiO_2$ for sensing purposes, have been demonstrated.*

UNIVERSITY OF
EASTERN FINLAND

*uef.fi*

**PUBLICATIONS OF**
**THE UNIVERSITY OF EASTERN FINLAND**
*Dissertations in Forestry and Natural Sciences*

ISBN 978-952-61-3036-1
ISSN 1798-5668